Eur Spine J (2014) 23:328–336
DOI 10.1007/s00586-013-2963-6

ORIGINAL ARTICLE

The O-C2 angle established at occipito-cervical fusion dictates the patient's destiny in terms of postoperative dyspnea and/or dysphagia

Masanori Izeki · Masashi Neo · Mitsuru Takemoto · Shunsuke Fujibayashi · Hiromu Ito · Koutatsu Nagai · Shuichi Matsuda

Received: 13 December 2012 / Revised: 14 June 2013 / Accepted: 6 August 2013 / Published online: 25 August 2013

Abstract

Purpose We have revealed that the cause of postoperative dyspnea and/or dysphagia after occipito-cervical (O-C) fusion is mechanical stenosis of the oropharyngeal space and the O-C2 alignment, rather than total or subaxial alignment, is the key to the development of dyspnea and/or dysphagia. The purpose of this study was to confirm the impact of occipito-C2 angle (O-C2A) on the oropharyngeal space and to investigate the chronological impact of a fixed O-C2A on the oropharyngeal space and dyspnea and/or dysphagia after O-C fusion.

Materials and methods We reviewed 13 patients who had undergone O-C2 fusion, while retaining subaxial segmental motion (OC2 group) and 20 who had subaxial fusion without O-C2 fusion (SA group). The O-C2A, C2–C6 angle and the narrowest oropharyngeal airway space were measured on lateral dynamic X-rays preoperatively, when dynamic X-rays were taken for the first time postoperatively, and at the final follow-up. We also recorded the current dyspnea and/or dysphagia status at the final follow-up of patients who presented with it immediately after the O-C2 fusion.

Results There was no significant difference in the mean preoperative values of the O-C2A (13.0 ± 7.5 in group OC2 and 20.1 ± 10.5 in group SA, Unpaired t test, $P = 0.051$) and the narrowest oropharyngeal airway space (17.8 ± 6.0 in group OC2 and 14.9 ± 3.9 in group SA, Unpaired t test, $P = 0.105$). In the OC2 group, the narrowest oropharyngeal airway space changed according to the cervical position preoperatively, but became constant postoperatively. In contrast, in the SA group, the narrowest oropharyngeal airway space changed according to the cervical position at any time point. Three patients who presented with dyspnea and/or dysphagia immediately after O-C2 fusion had not resolved completely at the final follow-up. The narrowest oropharyngeal airway space and postoperative dyspnea and/or dysphagia did not change with time once the O-C2A had been established at O-C fusion.

Conclusions The O-C2A established at O-C fusion dictates the patient's destiny in terms of postoperative dyspnea and/or dysphagia. Surgeons should pay maximal attention when establishing the O-C2A during surgery, because their careless decision for the O-C2A may cause persistent dysphagia or a life-threatening consequence. We recommend that the O-C2A in O-C fusion should be kept at least at more than the preoperative O-C2A in the neutral position.

Keywords Upper airway · Cervical fusion · Cervical alignment · Dysphagia · Complication

M. Izeki · M. Takemoto · S. Fujibayashi · H. Ito · S. Matsuda
Department of Orthopaedic Surgery, Graduate School of Medicine, Kyoto University, Kyoto, Japan

M. Neo (✉)
Department for Orthopedic Surgery, Osaka Medical College, 2-7 Daigaku-machi, Takatsuki, Osaka 569-8686, Japan
e-mail: neo@kuhp.kyoto-u.ac.jp; neo@poh.osaka-med.ac.jp

K. Nagai
Department of Physical Therapy, Faculty of Health Science, Kyoto Tachibana University, Kyoto, Japan

Introduction

Postoperative dyspnea and/or dysphagia (D/D) after occipito-cervical (O-C) fusion are rare but pose an obstacle

to activities of daily living and are occasionally life-threatening [1–4]. Although, the true cause of D/D has not been elucidated, cervical flexed alignment has been thought to be a major factor, in addition to pharyngeal edema or a postoperatively enlarged tongue [5–7].

However, we have revealed that the cause of postoperative D/D after O-C fusion is mechanical stenosis of the oropharyngeal space and the O-C2 alignment alone, and not total cervical alignment or subaxial alignment, is the key to the development of D/D. Miyata et al. [8] showed that reduction of the O-C2 angle (O-C2A) after O-C fusion was associated with postoperative D/D, and demonstrated that the O-C2A had a great impact on D/D and the oropharyngeal space, where both respiratory and swallowing functions are involved. They demonstrated that if the O-C2A was reduced by more than 10° compared with the preoperative neutral position, all patients developed D/D after surgery. Ota et al. [9] investigated the association between cervical alignment and the oropharyngeal space in normal volunteers. They demonstrated that the narrowest oropharyngeal airway space (nPAS) was strongly associated with the O-C2A, whereas the C2–C6 angle (C2–C6A) was not significantly associated with the nPAS. They also showed that a decrease in the O-C2A of 10° caused a reduction of the nPAS in the neutral position of approximately 37 %.

The mechanism of postoperative oropharyngeal stenosis caused by a reduction in the O-C2A has been speculated to be as follows (Fig. 1). Soft tissue surrounds the oropharyngeal space, of which the anterior tongue root is the largest component. This soft tissue is surrounded by bony structures: the mandible anteriorly and laterally and the cervical spine posteriorly. A reduction in the O-C2A makes the mandible shift posteriorly. This reduces the volume of the bony container around the oropharyngeal region, resulting in local airway stenosis [8–10]. A reduction in the oropharyngeal space causes dysphagia or, occasionally, dyspnea as a more severe form [8]. Research from another group has also supported our hypothesis. Ataka et al. [10] reported that obstructive sleep apnea in patients with rheumatoid arthritis (RA) with an upper cervical spine lesion improved after O-C fusion when the O-C2A was fixed in a more extended position, because it caused enlargement of the oropharyngeal space.

Given this background, we hypothesized that the oropharyngeal space or nPAS, once established by O-C2 fusion, will not change according to the cervical position at any postoperative point, so that any D/D occurring after O-C fusion cannot be resolved. On the other hand, in subaxial fusion procedures that retain O-C2 segmental motion, the postural change of the oropharyngeal space should be maintained for all cervical positions at all postoperative time.

All previous studies focused on the changes in the O-C2A and oropharyngeal space just after the surgery or after a short follow-up period, and also followed the patient's D/D status after the O-C fusion for a short time only [8, 10]. As far as we know, no study has assessed the chronological changes in the oropharyngeal space established at the O-C fusion, or in postoperative D/D status. Therefore, one of the aims of this study was to establish these outcomes for patients undergoing subaxial fusion as a control group. Another objective was to investigate the current D/D status of those patients who presented with D/D immediately after the O-C2 fusion.

Materials and methods

Our hospital's institutional review board approved this study.

As a study group, 16 patients who underwent posterior O-C2 fusion surgery while retaining subaxial cervical motion at our institution from April 1997 to September 2010, using a rigid occipital plate and a screw–rod system, were reviewed retrospectively. O-C2 fusions using a semirigid fixation technique, such as wiring, were excluded from this study, since some change in the O-C2A might have occurred before bone union was completed. Three patients were excluded from this study because one lacked postoperative dynamic lateral X-rays and two could not be followed for more than 1 year. The cases finally analyzed were the remaining 13 patients who underwent O-C2 fusion (OC2 group: 6 men and 7 women; mean age 61.2 years; range from 29 to 84 years). The diagnoses included RA ($n = 9$), O-C1 assimilation ($n = 3$), destructive spondyloarthropathy ($n = 1$).

As a control group, 38 patients who received subaxial fusion surgery during the same period including anterior and/or posterior cervical spinal fusion (ACF and/or PCF) without O-C2 fusion were reviewed. We defined this group as comprising patients having continuous fusion from C2 or C3 as the most cranial vertebra to C6 or below as the most distal vertebra. Eighteen patients were excluded from this study because of absent or inadequate imaging studies ($n = 13$), or a follow-up of less than 1 year ($n = 5$). This resulted in a group of 20 patients with subaxial fusion (SA group: 11 men and 9 women; mean age 64.6 years; range from 44 to 80 years). In the SA group, original diagnoses included nonunion after ACF ($n = 3$), cervical spondylotic myelopathy ($n = 9$), destructive spondyloarthropathy ($n = 3$), cervical spondylotic amyotrophy ($n = 2$), RA ($n = 1$), ossification of the posterior longitudinal ligament ($n = 1$), and a tumor ($n = 1$). The fused levels were as follows: C2–6 ($n = 4$), C2–7 ($n = 3$), C2–Th1 ($n = 1$), C3–6 ($n = 8$), C3–7 ($n = 3$), and C3–Th1 ($n = 1$). The

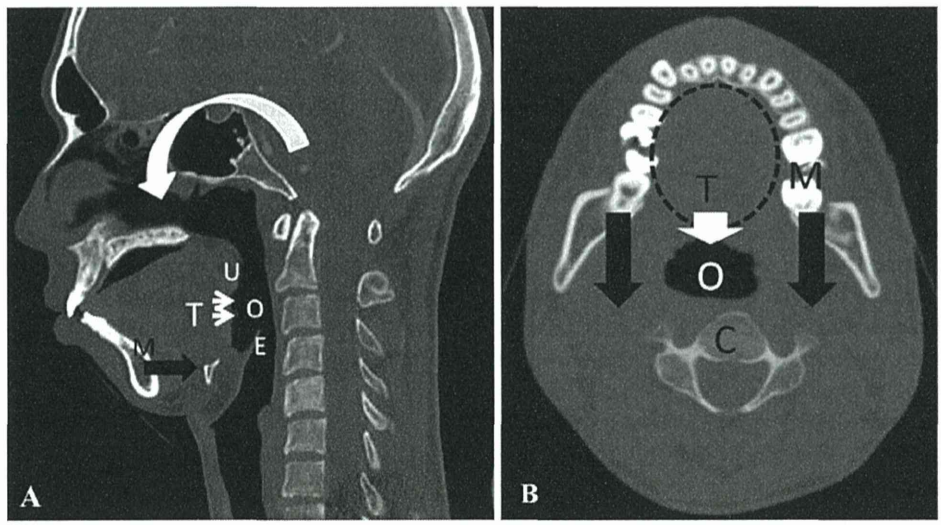

Fig. 1 Schematic drawing of the proposed mechanism of oropharyngeal stenosis. *U* uvula, *E* epiglottis, *M* mandible, *T* tongue root, *O* oropharynx, *C* cervical spine. **a** Sagittal computed tomography reconstruction of the cervical spine. Reduction in the O-C2A flexes the maxilla (*curved white arrow*), which makes the mandible shift posteriorly (*black arrow*) with the tongue root (*thin white arrows*). **b** Movement of the tongue root (*while arrow*) caused by the backward shift of the mandible (*black arrow*) results in oropharyngeal stenosis

mean number of fused levels was 3.9 (range 3–6). ACF was performed in 6 cases, PCF was done in 8 cases, and the remaining 6 patients underwent combined ACF and PCF.

Patients were excluded if they had preoperative dysphagia, dyspnea, and dysphonia in both groups. The mean follow-up period was 45 months (range from 13 to 72 months) in the OC2 group and 52.3 months (range from 12 to 120 months) in the SA group.

Radiographic assessment

We reviewed dynamic lateral plain X-rays to measure O-C2A, C2–C6A and the nPAS preoperatively, when dynamic X-rays were taken for the first time postoperatively (a mean of 8.8 months after the operation in the OC2 group and a mean of 12.2 months in the SA group), and at the final follow-up.

The O-C2A, C2–C6A, and nPAS parameters have been documented elsewhere [9, 11]. Briefly, the O-C2A indicates the angle between McGregor's line and the inferior vertebral endplate line of C2. C2–C6A indicates the angle between the inferior endplates of the C2 and C6 vertebral bodies. If the C6 vertebra had been included in an ACF procedure, we used the C2–C7 angle for analysis. In both measurements, a positive value indicates lordosis at the local segment. The nPAS was defined as the shortest anteroposterior distance from the posterior pharyngeal wall to the back of the tongue between the levels of the uvula tip and the tip of the epiglottis (Fig. 2) [9].

The difference in the O-C2A (dOC2A), that is the differences between the values in the flexion or extension (X position) and the value in the neutral position, was calculated for each cervical position (flexion or extension) at each time point.

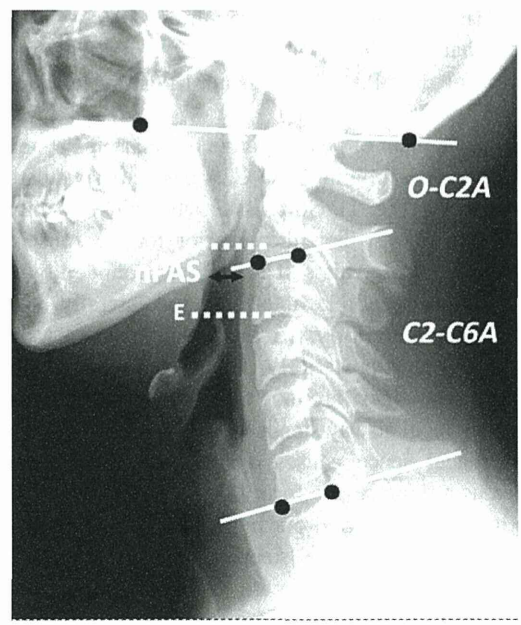

Fig. 2 Representative radiographic measurements. *E* epiglottis tip, *U* uvula tip. The *O-C2A* represents the angle between McGregor's line and the inferior endplate of C2. The *C2–C6A* represents the angle between the inferior endplates of C2 and C6. In both, a positive value indicates lordosis at the local segment. '*nPAS*' represents the narrowest anteroposterior distance of the oropharynx between the tips of the uvula and epiglottis (*double black arrow*)

$$\text{dOC2A } (^\circ) = (\text{O-C2A in the X position}) - (\text{O-C2A in the neutral position})$$

To normalize data for the variability of patients in terms of the pharyngeal space, the difference in the nPAS according to each cervical position (%dnPAS) was calculated from the following formula:

$$\%\ \text{dnPAS } (\%) = (\text{nPAS in the X position} - \text{nPAS in the neutral position})/(\text{nPAS in the neutral position}) \times 100.$$

We represented the maximal amount of postural change of the nPAS at each time point as Δ nPAS. This was defined as the following formula:

$$\Delta\text{nPAS (mm)} = (\text{maximal nPAS} - \text{minimal nPAS}).$$

The maximal and minimal values were chosen among the three different positions: neutral, flexion, or extension at each time point. We calculated the ΔO-C2A and ΔC2–C6A values using a similar formula. All linear and angular parameters were calculated with a precision of 0.1 mm and 0.1° using the Centricity PACS system (version 2.0; GE Healthcare, Milwaukee, WI, USA).

Clinical assessment

We investigated the occurrence of postoperative D/D in both groups, and interviewed at the final follow-up who presented with D/D immediately after the operation about the severity of the swallowing difficulty. All of them were asked to select one of three replies about their subjective D/D status: improved, unchanged, or deteriorated compared with shortly after the operation.

Statistical analysis

Values are expressed as the mean ± standard deviation. Differences in baseline characteristics were tested using Student's t test for continuous variables and with the χ^2 test for categorical variables. Nonnormally distributed variables were compared using the Mann–Whitney nonparametric U test. Spearman correlation coefficients (ρ) were used to evaluate any associations between dOC2A and %dnPAS. Differences in variation of the ΔnPAS in both groups were analyzed using an analysis of covariance (ANCOVA), and the Wilcoxon signed-rank test with Bonferroni's correction. $P < 0.05$ was considered statistically significant. We used SPSS software (version12.0; SPSS Inc., Chicago, IL, USA) for all analyses.

Results

The excellent reproducibility and repeatability of the O-C2A, C2–C6A, and nPAS parameters measured on lateral cervical X-rays have been documented elsewhere [9, 11]. Briefly, the radiographs were measured twice with a 1-week interval by the same 2 spine surgeons, independently. Reliability was evaluated by calculating the intraclass correlation coefficient (ICC). The inter- and intraobserver ICCs values of the radiographic parameters for all cervical positions were more than 0.93.

The patient's demographic data for both groups are shown in Table 1. There were no significant differences between the two groups in terms of age, male-to-female ratio, or mean follow-up period.

Preoperative morphological measurements data are shown in Table 2. There was significant difference between the 2 groups only in ΔO-C2A value, reflecting the fact that the cases in the OC2 group had upper cervical lesions.

Figure 3 shows the association between the dOC2A and %dnPAS preoperatively and at the final follow-up. In the OC2 group, the preoperative scatter diagram shows that there was a positive linear correlation (Fig. 3a: Spearman's $\rho = 0.75$, $P < 0.001$), whereas no significant correlation was found in the final follow-up (Fig. 3b: Spearman's $\rho = 0.014$, $P = 0.947$). The %dnPAS became constant compared with its preoperative distribution, even though the C2–C6 motion was preserved. In the SA group, a strong positive linear correlation of dOC2A with %dnPAS was found at both time points (preoperative: Spearman's $\rho = 0.70$, $P < 0.001$; final follow-up: Spearman's $\rho = 0.88$, $P < 0.001$; Fig. 3c, d).

Figure 4 shows chronological changes in the ΔnPAS. The ΔnPAS value in the OC2 group at the first postoperative point and at the final follow-up was significantly smaller than preoperatively ($P = 0.002$), and there was no significant difference between the first postoperative point and the final follow-up ($P = 0.1$). On the other hand, there were no significant differences in the value of ΔnPAS among preoperative, postoperative, and the final follow-up points in the SA group. These findings demonstrate that the postural change in nPAS diminished dramatically, and became constant once the O-C2 is fixed. A representative case in each group is presented in Fig. 5.

In clinical assessment, although 2 patients in the control group complained of swallowing difficulty after ACF only in the early postoperative period, no patient had subjective dysphagia at the final follow-up. In the study group, 3 patients had D/D immediately after the O-C fusion and continued to the final follow-up (Table 3), and the remaining 10 patients had not complained of D/D through

Table 1 Summary of patients demographic data (mean ± SD)

	Group OC2	Group SA	*P*
Case number	13	20	
Sex male:female	6:7	11:9	0.728[a]
Mean age (years)	61.2 ± 15.2	64.6 ± 9.3	0.522[b]
Term to the first dynamic X-rays since operation (m)	8.8 ± 2.4	12.2 ± 7.0	0.171[b]
Final F/U (m)	45.0 ± 18.6	52.3 ± 32.0	0.512[b]
Diagnosis	RA ($n = 9$)	CSM ($n = 9$), nonunion after ACF ($n = 3$),	
	O-C1 assimilation ($n = 3$)	DSA ($n = 3$), CSA ($n = 2$), RA ($n = 1$)	
	DSA ($n = 1$)	OPLL ($n = 1$), tumor ($n = 1$)	

Final F/U final follow-up, *RA* rheumatoid arthritis, *DSA* destructive spondyloarthropathy, *CSM* cervical spondylotic myelopathy, *ACF* anterior cervical spinal fusion, *CSA* cervical spondylotic amyotrophy, *OPLL* ossification of the posterior longitudinal ligament

[a] χ^2 test

[b] Mann–Whitney *U* test

Table 2 Preoperative morphological measurements (mean ± SD)

	OC2 group	SA group	*P*
O-C2A (°)	13.0 ± 7.5	20.1 ± 10.5	0.051[a]
ΔO-C2A (°)	13.9 ± 9.2	26.2 ± 9.4	0.001[a]*
C2–C6A (°)	12.8 ± 9.5	5.7 ± 14.0	0.131[a]
ΔC2–C6A (°)	31.3 ± 12.9	29.9 ± 13.1	0.771[a]
nPAS (mm)	17.8 ± 6.0	14.9 ± 3.9	0.105[a]
ΔnPAS (mm)	7.0 ± 5.1	9.7 ± 4.9	0.169[b]

ΔnPAS = (maximal nPAS − minimal nPAS). The maximal and minimal values were chosen from among the three different positions: neutral, flexion, or extension

O-C2A occipito-C2 angle, *C2-C6A* C2-C6 angle, *nPAS* represents the narrowest anteroposterior distance of the oropharynx

* Statistically significant

[a] Unpaired *t* test

[b] Mann–Whitney *U* test

the whole postoperative period. For these D/D patients, we consulted to otolaryngologists as for postoperative D/D pathology. They performed routine examination of laryngopharynx (3 patients), laryngoscopy (2 patients), and esophagography (1 patient). However, no neurological or mucosal pathology were pointed out. All patients did not desire further confirmatory test or treatment for dysphagia, because their symptom was mild.

Discussion

We have argued that the main cause of postoperative D/D after the O-C fusion is fixation with an O-C2A that is smaller than the preoperative neutral position [8]. The absolute value of the O-C2A in a neutral position varies between individuals, and any change from this position is important clinically [9, 12, 13]. The impact of the O-C2A on the oropharyngeal space and D/D after the O-C fusion has been demonstrated from several directions [8–10], and the present study reconfirms it clearly from another perspective. Furthermore, we clarified that the nPAS and postoperative D/D did not change with time once the O-C2A had been established during the O-C fusion.

It is well known that dysphagia sometimes occurs after ACF. Proposed causes include pharyngeal edema, transient local nerve palsy, use of plate fixation, plate prominence, the use of recombinant human bone morphogenetic protein-2, and severe pain [14–18]. The incidence of dysphagia was reported to be 50–56% at 1 month after ACF, but the symptoms resolved gradually over the first few months. At 1 year, only 13–21% of patients were symptomatic [14, 19]. Since the mechanism of dysphagia after the O-C fusion is speculated to be quite different from that after ACF, spontaneous recovery is much less likely, that is, the cause of D/D after the O-C fusion is mainly mechanical stenosis of the airway and it occurs regardless of inflammation, edema, or neuropraxia. Therefore, it should be stressed that once D/D occurs after the O-C fusion, and if the fixed O-C2A is found to be smaller than that in the preoperative neutral position, the surgeon should not hesitate to correct the O-C2A to the preoperative neutral position or slightly more. It would be unfortunate, if the surgeon were to wait for several months, expecting spontaneous recovery, in which time bone union was completed. After the publication of our previous papers [8, 9], we were consulted regarding 2 cases of postoperative dysphagia from other hospitals. We recommended correction of the O-C2 alignment based on measuring the O-C2A. The dysphagia disappeared immediately after the revision surgery in both cases. As Ota et al. [9] demonstrated, a decrease in the O-C2A of only 10° caused a reduction of approximately 37% in the nPAS at the neutral position. This means that even a slight change in the O-C2A will dramatically affect the oropharyngeal space.

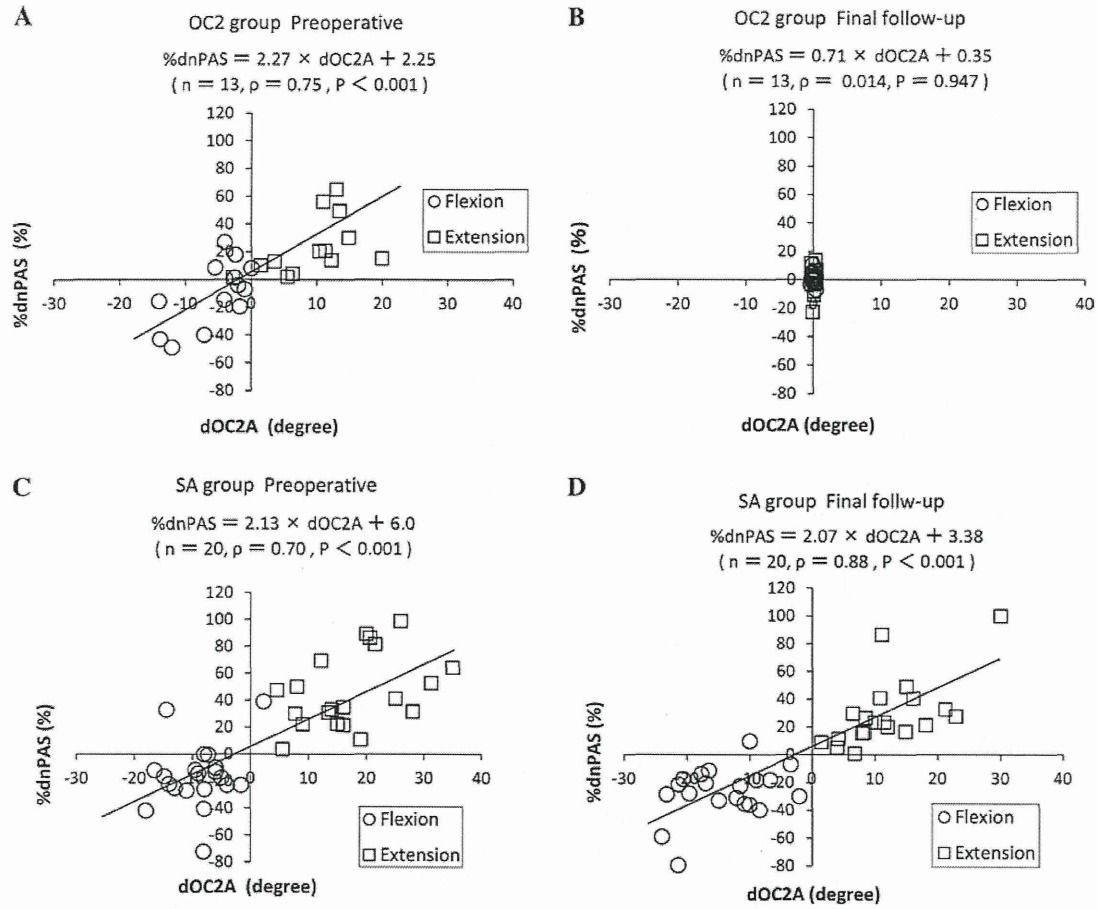

Fig. 3 A *scatter diagram* showing the association between the dOC2A and the %dnPAS. dOC2A (°) = (O-C2A in the X position) − (O-C2A in the neutral position). %dnPAS (%) = (nPAS in the X position − nPAS in the neutral position)/(nPAS in the neutral position) × 100. '*X position*' indicates flexion or extension. **a** OC2 group: preoperative values. **b** OC2 group: final follow-up values. **c** SA group: preoperative values. **d** SA group: final follow-up values

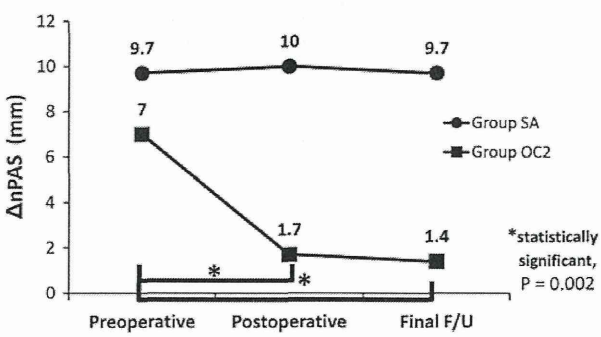

Fig. 4 This *line graph* shows the chronological changes in the ΔnPAS between the 2 groups. *Final F/U* final follow-up, *statistically significance

Recent refinements in instrumentation, such as the plate–screw–rod system, and the advent of strong anchoring techniques, such as Magerl or pedicle screws, have enabled us to obtain very rigid fixation with excellent clinical results. However, these systems do not allow for slight postoperative changes in the O-C2A, probably decreasing the chance of a spontaneous recovery from D/D after the O-C fusion. In the conventional semirigid fixation techniques, such as onlay bone grafting with halo-vest fixation or sublaminar segmental wiring techniques, it is possible that postoperative D/D will improve spontaneously by allowing the patient to achieve unconscious adjustment of the fixed position. Therefore, the O-C2A determined during surgery might now be the most important factor in avoiding postoperative D/D.

The present study had several weaknesses and limitations, including its retrospective study design, and relatively small sample size with many cases being excluded. Another limitation of our study is that dysphagia is a subjective manifestation, so different individuals might view even the same condition differently, and some cases might be underreported [20]. Therefore, in the absence of universal questionnaires to evaluate the degree of

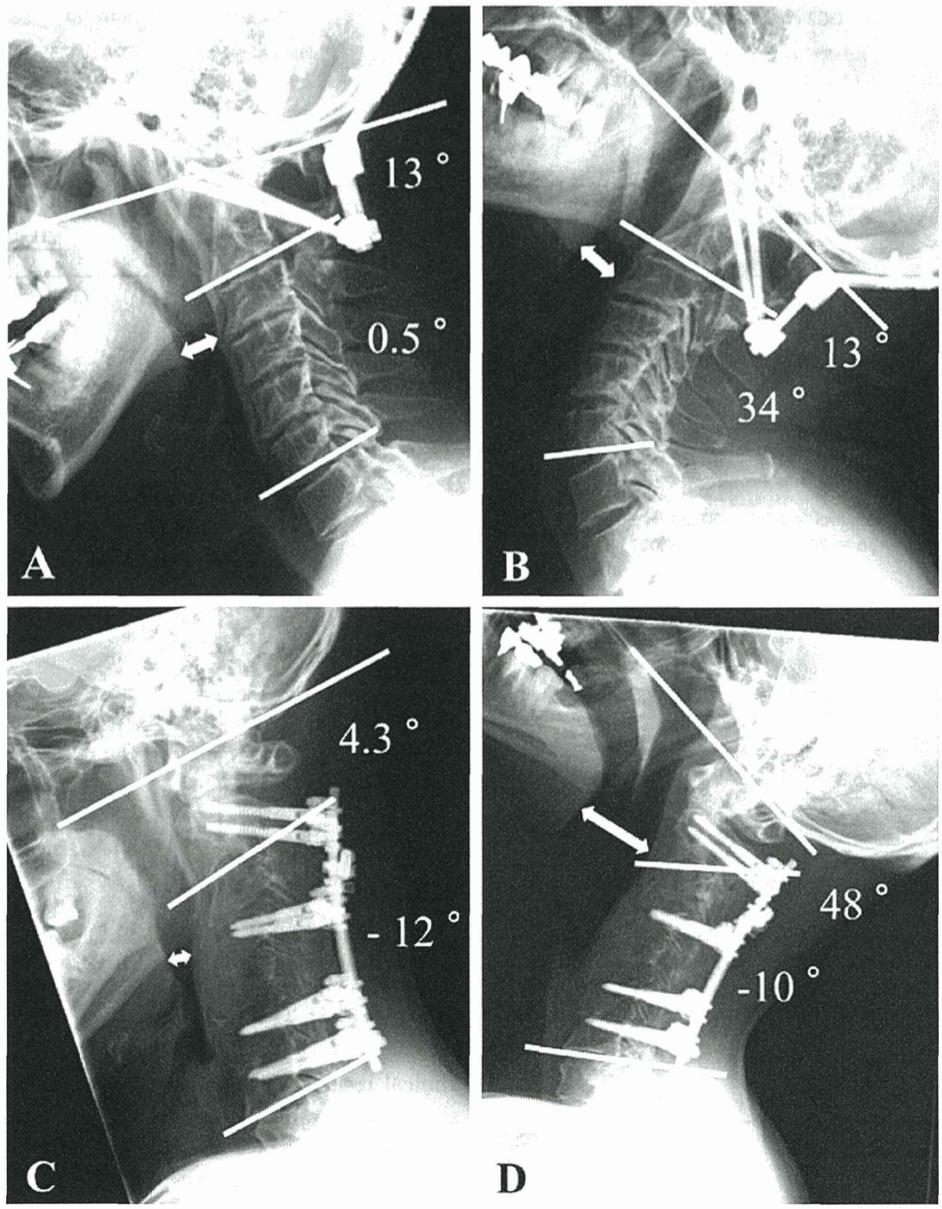

Fig. 5 Postoperative lateral radiographs in the flexion and extension (**a**, **b**). A case in the OC2 group. The nPAS (*double white arrow*) became almost constant, once the O-C2A had been fixed (nPAS: 14.2 mm in flexion, and 15.4 mm in extension) (**c**, **d**). A case with C2–C7 posterior cervical fusion in the SA group. The changes in the nPAS had been maintained even after subaxial fusion (nPAS: 5.3 mm in flexion, and 32.9 mm in extension)

dysphagia in patients undergoing cervical spine surgery, it is best to evaluate the swallowing function objectively both pre- and postoperatively, for example using the Bazaz grading system and Dysphagia Short Questionnaire [15, 21]. Another limitation of this study was the difference between groups in the ratio of patients with RA, because it has been recognized that RA is a major risk factor for postoperative narrowing of the airway [22–24]. However, it has been speculated that mechanical stenosis caused by upper cervical alignment also plays a major role in postoperative airway complications in such patients [10, 25].

Considering the ease of exposure of the operative field, we might generate a flexed position of the O-C2A during the surgery. Moreover, it is very difficult to notice slight changes in the O-C2 alignment macroscopically. Therefore, the surgeon must check the O-C2A using a C-arm after the insertion of all cervical screws and, if necessary,

Table 3 Summary of data of 3 patients with dyspnea and/or dysphagia after O-C2 fusion

Case no.	Age (years), sex	Origin	Fusion range	FU (m)	O-C2A variation (°)[a]	Pre-op nPAS[b] (mm)	Post-op nPAS[b] (mm)	Final F/U nPAS[b] (mm)	Complications	Outcome of the sequelae
1.	41, M	O-C1 As, AAS	O-C2	84	−14	12.3	10.0	10.7	Dysphagia	No change
2.	56, F	RA, AAS, VS	O-C2	51	−16	16.8	8.5	9.8	Dysphagia	No change
3.	73, F	DSA	O-C2	35	−6.5	12.4	8.8	12.0	Dysphagia	Continued but slightly improved

O-C1 As O-C1 assimilation, *RA* rheumatoid arthritis, *AAS* atlantoaxial subluxation, *VS* vertical subluxation, *DSA* destructive spondyloarthropathy

[a] O-C2A variation = (postoperative O-C2A in the neutral position) − (preoperative O-C2A in the neutral position)

[b] Measurement in the neutral position

change the patient's head position just before the final occipital plate-rod fixation.

Surgeons should be aware that the O-C2A established at the O-C fusion dictates the patient's destiny in terms of postoperative D/D and should pay full attention when establishing it during the surgery. Furthermore, they should not hesitate to correct the O-C2A should they encounter D/D in a patient after the O-C fusion with a reduced O-C2A.

Acknowledgments The authors are grateful to all the staff of the Kyoto University for allowing them to study their patients and for their assistance.

Conflict of interest No benefits in any form have been or will be received from a commercial party related directly or indirectly to the subject of this paper.

References

1. Matsuyama Y, Kawakami N, Yoshihara H et al (2005) Long-term results of occipitothoracic fusion surgery in RA patients with destruction of the cervical spine. J Spinal Disord Tech 18(suppl 1):S101–S106
2. Tagawa T, Akeda K, Asanuma Y et al (2011) Upper airway obstruction associated with flexed cervical position after posterior occipitocervical fusion. J Anesth 25(1):120–122
3. Yoshida M, Neo M, Fujibayashi S, Nakamura T (2007) Upper-airway obstruction after short posterior occipitocervical fusion in a flexed position. Spine (Phila Pa 1976) 32(8):E267–E270
4. Ichinose K, Kozuma S, Fukuyama S et al (2002) A case of airway obstruction after posterior occipito-cervical fusion (in Japanese). Masui 51(5):513–515
5. Meakem TD, Meakem TJ, Rappaport W (1990) Airway compromise from prevertebral soft tissue swelling during placement of halo-traction for cervical spine injury. Anesthesiology 73(4):775–776
6. Dark A, Armstrong T (1999) Severe postoperative laryngeal oedema causing total airway obstruction immediately on extubation. Br J Anaesth 82(4):644–646
7. Lee YH, Hsieh PF, Huang HH, Chan KC (2008) Upper airway obstruction after cervical spine fusion surgery: role of cervical fixation angle. Acta Anaesthesiol Taiwan 46(3):134–137
8. Miyata M, Neo M, Fujibayashi S et al (2009) O-C2 angle as a predictor of dyspnea and/or dysphagia after occipitocervical fusion. Spine (Phila Pa 1976) 34(2):184–188
9. Ota M, Neo M, Aoyama T et al (2011) Impact of the O-C2 angle on the oropharyngeal space in normal patients. Spine (Phila Pa 1976) 36(11):E720–E726
10. Ataka H, Tanno T, Miyashita T, Isono S, Yamazaki M (2010) Occipitocervical fusion has potential to improve sleep apnea in patients with rheumatoid arthritis and upper cervical lesions. Spine (Phila Pa 1976) 35(19):E971–E975
11. Izeki M, Neo M, Ito H et al (2013) Reduction of atlantoaxial subluxation causes airway stenosis. Spine (Phila Pa 1976) 38(9):E513–E520
12. Shoda N, Takeshita K, Seichi A et al (2004) Measurement of occipitocervical angle. Spine (Phila Pa 1976) 29(10):E204–E208
13. Matsunaga S, Onishi T, Sakou T (2001) Significance of occipitoaxial angle in subaxial lesion after occipitocervical fusion. Spine (Phila Pa 1976) 26(2):161–165
14. Lee MJ, Bazaz R, Furey CG, Yoo J (2007) Risk factors for dysphagia after anterior cervical spine surgery: a two-year prospective cohort study. Spine J 7(2):141–147
15. Bazaz R, Lee MJ, Yoo JU (2002) Incidence of dysphagia after anterior cervical spine surgery: a prospective study. Spine (Phila Pa 1976) 27(22):2453–2458
16. Riley LH 3rd, Skolasky RL, Albert TJ, Vaccaro AR, Heller JG (2005) Dysphagia after anterior cervical decompression and fusion: prevalence and risk factors from a longitudinal cohort study. Spine (Phila Pa 1976) 30(22):2564–2569
17. Vaidya R, Weir R, Sethi A et al (2007) Interbody fusion with allograft and rh-BMP-2 leads to consistent fusion but early subsidence. J Bone Joint Surg Br 89(3):342–345
18. Haller JM, Iwanik M, Shen FH (2011) Clinically relevant anatomy of high anterior cervical approach. Spine (Phila Pa 1976) 36(25):2116–2121
19. Riley LH 3rd, Vaccaro AR, Dettori JR, Hashimoto R (2010) Postoperative dysphagia in anterior cervical spine surgery. Spine (Phila Pa 1976) 35(9 Suppl):S76–S85
20. Edwards CC 2nd, Karpitskaya Y, Cha C et al (2004) Accurate identification of adverse outcome after cervical spine surgery. J Bone Joint Surg Am 86(2):251–256
21. Martin S, Catarina I, Therese E, Claes O (2012) The dysphagia short questionnaire: an instrument for evaluation of dysphagia—a validation study with 12 months' follow-up after anterior cervical spine surgery. Spine (Phila Pa 1976) 37(11):996–1002
22. Redlund-Johnell I (1988) Upper airway obstruction in patients with rheumatoid arthritis and temporomandibular joint destruction. Scand J Rhumatol 17(4):273–279

23. Keenan MA, Stiles CM, Kaufman RL (1983) Acquired laryngeal deviation associated with cervical spine disease in erosive polyarticular arthritis. Use of the fiberoptic bronchoscope in rheumatoid disease. Anesthesiology 58(5):441–449
24. Chen JJ, Branstetter BF 4th, Myers EN (2005) Cricoarytenoid rheumatoid arthritis: an important consideration in aggressive lesions of the larynx. AJNR Am J Neuroradiol 26(4):970–972
25. Ataka H, Isono S, Yamazaki M, Tanno T, Miyashita T (2011) Sleep-disordered breathing in patients with rheumatoid arthritis and upper cervical lesion (in Japanese). J Spine Res 2(1):35–42

RNAi-induced loss of *pat-10* disrupts endocytosis through impairment of the actin cytoskeleton (*12*, *13*, *15*). To assay the role of *pat-10* in endocytosis, we used a secretion and endocytosis reporter designed to actively secrete GFP (ssGFP) from muscle cells into the pseudocoelomic fluid, where it is endocytosed by the coelomocyte cells and degraded (fig. S9A) (*16*). Therefore, the ssGFP reports upon effective muscular secretion and endocytosis by coelomocytes. Fitting the hypothesis that *pat-10* overexpression improves transport and cellular processing through improved subcellular scaffolding, the *pat-10 OE* strain had a decrease in overall ssGFP fluorescence (Fig. 3, E and F). The decrease in ssGFP resulted from improved secretion and uptake, as shown by the absence of fluorescence in the muscle and pseudocoelomic fluid (Fig. 3E). This decrease was not due to an overall decrease in expression of GFP (fig. S9B). Conversely, RNAi of *pat-10* increased overall fluorescence through decreased muscle secretion and coelomocytic endocytosis (Fig. 3, E and G). To fully block coelomocytic uptake and degradation of ssGFP, RNAi of *cup-4*, a ligand-gated ion channel required in endocytosis (*17*), showed an even higher increase in fluorescence (Fig. 3G) and also reduced thermotolerance in the wild type (Fig. 3H). Collectively, these data indicate *pat-10* has an active role in cytoskeletal maintenance, which is critical to cellular transport.

To test for conservation, we disrupted the actin cytoskeleton in human embryonic kidney (HEK) 293T cells using cytochalasin D, which blocks the addition of actin monomers to filaments (*18*), or latrunculin A, which binds actin monomers and prevents polymerization (Fig. 4A) (*19*). Inhibiting filamentous actin formation with either cytochalasin D or latrunculin A significantly reduced thermotolerance in human cells without causing death at permissive temperatures (Fig. 4B and fig. S10). Similar to our *C. elegans* data, these findings reiterate the importance of the actin cytoskeleton during times of cellular stress.

Elevated levels of *hsf-1* have been shown to benefit multiple organisms, yet its oncogenic properties are a major therapeutic drawback (*20*, *21*). Because the inducible chaperone network promotes survival and proliferation of metastasizing cells (*22*), the ability to harness protective, non-chaperone components within the HSF-1 signal transduction cascade appears essential for future drug development. Identification of *pat-10* as a modifier of thermotolerance and longevity may apply to mammalian systems without the typical oncogenic dangers associated with increased chaperone levels.

The *hsf-1(CT)* strain was still able to mount a transcriptional response to heat shock, albeit reduced in complexity of *hsf-1(FL)*. The molecular mechanism remains unclear by which *hsf-1(CT)* regulates transcription without the C-terminal activation domain, but possible explanations include HSF-1 containing multiple activation domains. Alternatively, the *hsf-1(CT)* modification may alter affinities to DNA-binding sites or different cofactors, which would modify the transcriptional profile.

Our findings underscore the importance of maintaining filamentous actin, as opposed to total levels of actin. We propose a model in which HSF-1 regulates chaperones and actin cytoskeletal genes in parallel to promote thermotolerance and longevity (Fig. 4C). In the absence of chaperone induction, stabilization of the actin cytoskeleton is sufficient to promote survival under conditions of cellular stress and aging.

REFERENCES AND NOTES

1. A.-L. Hsu, C. T. Murphy, C. Kenyon, *Science* **300**, 1142–1145 (2003).
2. M. Fujimoto *et al.*, *J. Biol. Chem.* **280**, 34908–34916 (2005).
3. G. McColl *et al.*, *Cell Metab.* **12**, 260–272 (2010).
4. N. Kourtis, V. Nikoletopoulou, N. Tavernarakis, *Nature* **490**, 213–218 (2012).
5. V. Prahlad, T. Cornelius, R. I. Morimoto, *Science* **320**, 811–814 (2008).
6. Y. M. Hajdu-Cronin, W. J. Chen, P. W. Sternberg, *Genetics* **168**, 1937–1949 (2004).
7. P. E. Kroeger, R. I. Morimoto, *Mol. Cell. Biol.* **14**, 7592–7603 (1994).
8. N. D. Trinklein, J. I. Murray, S. J. Hartman, D. Botstein, R. M. Myers, *Mol. Biol. Cell* **15**, 1254–1261 (2004).
9. H. Terami *et al.*, *J. Cell Biol.* **146**, 193–202 (1999).
10. K. Ono, S. Ono, *Mol. Biol. Cell* **15**, 2782–2793 (2004).
11. T. Obinata, K. Ono, S. Ono, *J. Cell Sci.* **123**, 1557–1566 (2010).
12. Z. Balklava, S. Pant, H. Fares, B. D. Grant, *Nat. Cell Biol.* **9**, 1066–1073 (2007).
13. T. Kuwahara *et al.*, *Hum. Mol. Genet.* **17**, 2997–3009 (2008).
14. L. A. Herndon *et al.*, *Nature* **419**, 808–814 (2002).
15. W. Greene, S.-J. Gao, *PLOS Pathog.* **5**, e1000512 (2009).
16. H. Fares, I. Greenwald, *Nat. Genet.* **28**, 64–68 (2001).
17. A. Patton *et al.*, *Curr. Biol.* **15**, 1045–1050 (2005).
18. J. F. Casella, M. D. Flanagan, S. Lin, *Nature* **293**, 302–305 (1981).
19. I. Spector, N. R. Shochet, Y. Kashman, A. Groweiss, *Science* **219**, 493–495 (1983).
20. L. Whitesell, S. Lindquist, *Expert Opin. Ther. Targets* **13**, 469–478 (2009).
21. C. H. Nguyen *et al.*, *Biochem. J.* **452**, 321–329 (2013).
22. D. R. Ciocca, A. P. Arrigo, S. K. Calderwood, *Arch. Toxicol.* **87**, 19–48 (2013).

ACKNOWLEDGMENTS

Bioinformatic analysis is included in the supplementary materials. The following funding sources supported this research: Howard Hughes Medical Institute, National Center for Research Resources (5P41RR011823-17), National Institute of General Medical Sciences (8 P41 GM103533-17), and National Institute on Aging (R01AG027463-04). N.A.B. was funded by a postdoctoral fellowship to the Salk Center for Nutritional Genomics from the Leona M. & Harry B. Helmsley Charitable Trust; P.M.D. was funded by George E. Hewitt Foundation for Medical Research and National Institute of Aging (1K99AG042495-01A1). We thank the laboratory of G. Lithgow for generously sharing the HSP-16 antibody and J. Durieux for helping design figure illustrations. Some of the nematode strains used in this work were provided by the *Caenorhabditis* Genetics Center (University of Minnesota), which is supported by the NIH–Office of Research Infrastructure Programs (P40 OD010440).

SUPPLEMENTARY MATERIALS

www.sciencemag.org/content/346/6207/360/suppl/DC1
Materials and Methods
Figs. S1 to S10
Tables S1
References (*23*–*40*)

10 March 2014; accepted 13 August 2014
10.1126/science.1253168

AUTOIMMUNITY

Detection of T cell responses to a ubiquitous cellular protein in autoimmune disease

Yoshinaga Ito,[1] Motomu Hashimoto,[1,2,3,4]* Keiji Hirota,[2]* Naganari Ohkura,[2,5] Hiromasa Morikawa,[2] Hiroyoshi Nishikawa,[2] Atsushi Tanaka,[2,5] Moritoshi Furu,[3,6] Hiromu Ito,[3,6] Takao Fujii,[3,4] Takashi Nomura,[1] Sayuri Yamazaki,[7] Akimichi Morita,[7] Dario A. A. Vignali,[8,9] John W. Kappler,[10,11] Shuichi Matsuda,[6] Tsuneyo Mimori,[4] Noriko Sakaguchi,[2] Shimon Sakaguchi[1,2,12]†

T cells that mediate autoimmune diseases such as rheumatoid arthritis (RA) are difficult to characterize because they are likely to be deleted or inactivated in the thymus if the self antigens they recognize are ubiquitously expressed. One way to obtain and analyze these autoimmune T cells is to alter T cell receptor (TCR) signaling in developing T cells to change their sensitivity to thymic negative selection, thereby allowing their thymic production. From mice thus engineered to generate T cells mediating autoimmune arthritis, we isolated arthritogenic TCRs and characterized the self antigens they recognized. One of them was the ubiquitously expressed 60S ribosomal protein L23a (RPL23A), with which T cells and autoantibodies from RA patients reacted. This strategy may improve our understanding of the underlying drivers of autoimmunity.

T cells mediate a variety of autoimmune diseases (*1*, *2*), likely through the recognition of self antigens. However, identification of the self antigens targeted by T cells in systemic autoimmune diseases such as rheumatoid arthritis (RA) has been technically difficult (*3*–*5*). This is because pathogenic T cells expressing high-affinity T cell receptors (TCRs) for ubiquitous self antigens may be largely deleted (i.e., negatively selected) in the thymus and

[1]Department of Experimental Pathology, Institute for Frontier Medical Sciences, Kyoto University, Kyoto 606-8507, Japan. [2]Department of Experimental Immunology, Immunology Frontier Research Center, Osaka University, Suita 565-0871, Japan. [3]Department of the Control for Rheumatic Diseases, Graduate School of Medicine, Kyoto University, Kyoto 606-8507, Japan. [4]Department of Rheumatology and Clinical Immunology, Graduate School of Medicine, Kyoto University, Kyoto 606-8507, Japan. [5]Department of Frontier Research in Tumor Immunology, Center of Medical Innovation and Translational Research, Osaka University, Osaka 565-0871, Japan. [6]Department of Orthopaedic Surgery, Graduate School of Medicine, Kyoto University, Kyoto 606-8507, Japan. [7]Department of Geriatric and Environmental Dermatology, Graduate School of Medical Sciences, Nagoya City University, Nagoya 467-8601, Japan. [8]Department of Immunology, St. Jude Children's Research Hospital, Memphis, TN 38105, USA. [9]Department of Immunology, University of Pittsburgh School of Medicine, Pittsburgh, PA 15261, USA. [10]Integrated Department of Immunology, National Jewish Health, Denver, CO 80206, USA. [11]Howard Hughes Medical Institute, National Jewish Health, Denver, CO 80206, USA. [12]Core Research for Evolutional Science and Technology (CREST), Japan Science and Technology Agency, Tokyo 102-0075, Japan. *These authors contributed equally to this work. †Corresponding author. E-mail: shimon@ifrec.osaka-u.ac.jp

scarcely detectable in the periphery or, if detected, in an inactivated state (*6*). This can be circumvented by altering TCR signaling, which changes the sensitivity of developing T cells to thymic selection and results in new dominant self-reactive TCR specificities that are causative of systemic autoimmune diseases (*7*–*11*). For example, a hypomorphic point mutation of ζ-associated protein 70 (ZAP-70), a TCR-proximal signaling molecule, causes T cell–mediated spontaneous autoimmune arthritis in mice, which resembles RA (*8*).

To identify ubiquitously expressed self antigens commonly targeted in mouse and human systemic autoimmune disease, we first examined whether the arthritogenic $CD4^+$ T helper (T_H) cells in BALB/c SKG mice, which develop autoimmune arthritis due to the ZAP-70 mutation, made use of a specific dominant TCR. We compared the arthritogenic capacity of SKG $CD4^+$ T cells expressing different TCR Vβ subfamilies (fig. S1). Transfer of SKG $CD4^+$ T cells expressing Vβ6, Vβ8.1/8.2, or Vβ10 into BALB/c *Rag2*$^{-/-}$ mice induced arthritis with similar severities. In addition, CDR3 gene segments of $V\beta6^+$ $CD4^+$ T cells in arthritic joints were diverse, with few common sequences among individual arthritic SKG mice (fig. S2 and tables S1 and S2). Thus, under the assumption that arthritogenic SKG $CD4^+$ T cells are highly polyclonal and make use of various Vα and Vβ TCR chains, we attempted to isolate a single arthritogenic $CD4^+$ T cell from a particular $CD4^+$ T cell subpopulation—for example, those expressing Vα2 and Vβ6, which constituted ~1% of joint-infiltrating $CD4^+$ T cells. To differentiate arthritogenic $CD4^+$ T cells from forkhead box P3 (Foxp3)–expressing $CD4^+$ regulatory T (T_{reg}) cells (*1*), we used SKG mice with knock-in of enhanced green fluorescent protein (EGFP)–Foxp3 fusion protein, designated eFOX SKG mice, which also spontaneously developed arthritis (fig. S3). We cloned a single TCR pair

A

Clone	Vα	Jα	CDR3	Vβ	Jβ	CDR3	Arthritogenic	Positive cells / Analyzed cells
1-23	14D-3/DV8*03	26*01	CAAS KG YAQGLTF	19*01	2-4*01	CASSI GGTGP SQNTLYF	No	1 / 12 (8.3%)
7-39	14D-3/DV8*03	40*01	CA AIY TGNYKYVF	19*01	2-1*01	CASS WRWGGER AEQFF	Yes	27 / 30 (90%)
6-39	14D-3/DV8*03	52*01	CAAS AA GANTGKLTF	19*01	2-7*01	CAS TPTF SYEQYF	Yes	2 / 26 (8%)

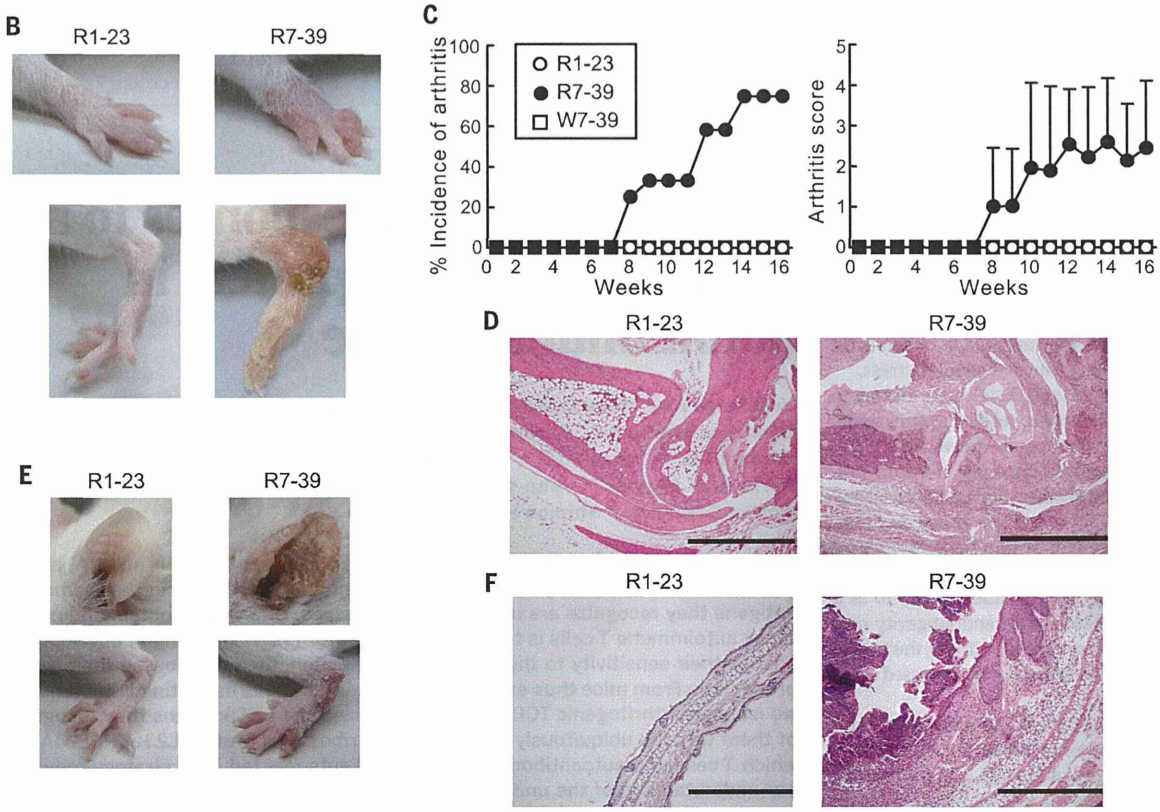

Fig. 1. Arthritis-inducing activity of two TCRs individually expressed in retrogenic mice. (**A**) Amino acid sequences and frequencies of two arthritogenic TCRs (7-39 and 6-39) and the nonarthritogenic 1-23 TCR. These three TCRs were obtained from three different mice. CDR, complementarity-determining region. Amino acid abbreviations: A, Ala; C, Cys; E, Glu; F, Phe; G, Gly; I, Ile; K, Lys; L, Leu; N, Asn; P, Pro; Q, Gln; R, Arg; S, Ser; T, Thr; V, Val; W, Trp; Y, Tyr. (**B**) Joint swelling in R7-39 retrogenic mice. (**C**) Incidence and scores of spontaneous arthritis in R7-39 (n = 11), R1-23 (n = 14), and W7-39 mice (n = 8). Error bars indicate means ± SD. (**D**) Hematoxylin and eosin (HE) staining of arthritic joints; scale bar, 1 mm. (**E**) Ears and hind paws of R7-39 and R1-23 mice. (**F**) HE staining of ears from R7-39 and R1-23 mice; scale bar, 500 μm. Results in (B) and in (D) to (F) represent three independent experiments.

from individual GFP$^-$ Vα2$^+$ Vβ6$^+$ CD4$^+$ T cells present in arthritic joints of eFOX SKG mice, transfected *Rag2*$^{-/-}$ SKG bone marrow (BM) cells with the TCR gene, and transferred the BM cells into *Rag2*$^{-/-}$ mice to construct retrogenic mice expressing the TCR pair in developing T cells (*12*–*15*). Among nine retrogenic strains each expressing a distinct TCR, those expressing 7-39 or 6-39 TCRs spontaneously developed arthritis at incidences of 80.0% and 27.3%, respectively (Fig. 1, A to C, and fig. S4, A to C). The two arthritogenic TCRs and a control nonarthritogenic 1-23 TCR used the same Vα and Vβ gene segments but different Jα and Jβ genes and CDR3 sequences (Fig. 1A). Arthritic joints in retrogenic 7-39 (R7-39) mice showed mononuclear cell infiltration, pannus formation, and cartilage destruction (Fig. 1D). Some (66.7%) of the R7-39, but not the R6-39, mice also developed chronic dermatitis, which exhibited hyperkeratosis and parakeratosis, histopathological features of human psoriasis (*16*) (Fig. 1, E and F, and fig. S5). Other organs were histologically intact (fig. S6).

In R7-39 mice, 7-39 TCR-transduced cells preferentially differentiated into monoclonal CD4$^+$ T cells with an activated and memory phenotype (fig. S7), and were able to transfer both arthritis and dermatitis into other *Rag2*$^{-/-}$ mice. Both arthritic R7-39 and nonarthritic R1-23 mice failed to develop Foxp3$^+$ T_{reg} cells (fig. S8). In contrast to 7-39 TCR gene-transfected *Rag2*$^{-/-}$ BM cells with the SKG ZAP-70 mutation, 7-39 TCR gene-transfected ZAP-70-intact *Rag2*$^{-/-}$ BALB/c BM cells did not cause arthritis in retrogenic mice (designated W7-39 mice). In W7-39 mice, the majority of 7-39 TCR-expressing CD4$^+$ T cells were negatively selected in the thymus, and those that had escaped thymic negative selection exhibited a naïve nonactivated phenotype, indicating their dormant or anergic state (Fig. 1C and fig. S9).

Taken together, these results demonstrate that CD4$^+$ T cells with a specific TCR mediate autoimmune arthritis and also dermatitis, and that more than one TCR specificity is individually able to confer T cell arthritogenicity.

We next constructed T cell hybridomas expressing 7-39 or 6-39 TCRs and attempted to determine the self antigens recognized by these TCRs. The 7-39 hybridoma cells produced interleukin-2 (IL-2) when stimulated by cell extracts not only from SKG fibroblast-like synoviocytes (FLSs) but also from P3U1 cells, a BALB/c plasma cell-derived cell line (fig. S10). In contrast, syngeneic antigen-presenting cells (APCs) were sufficient to induce IL-2 production by 6-39 hybridoma cells, indicating that the 6-39 TCRs recognized a self antigen constitutively displayed by APCs (fig. S4D). To further characterize the self antigen recognized by 7-39 TCRs, we reconstituted *Rag2*$^{-/-}$ mice with a mixture of 7-39 TCR-transfected *Rag2*$^{-/-}$ SKG BM cells and *TCR*β$^{-/-}$ BALB/c BM cells on the assumption that the autoantibodies produced by B cells might specifically react with the self antigen recognized by 7-39 TCRs because T cell help came solely from 7-39 T_H cells. The sera from these "B cell-reconstituted" mice specifically reacted with an 18-kD protein from the cell extract of P3U1 cells (Fig. 2A). Mass spectrometric analysis identified this protein as RPL23A, a component of the 60*S* subunit of ribosomes (*17*, *18*) (fig. S11). Various organs were found to express *RPL23A* mRNA at high levels (Fig. 2B). The amino acid sequence of RPL23A is 100% conserved between mice and humans (*18*). The sera from the B cell-reconstituted R7-39 mice indeed recognized recombinant RPL23A, but not histone H1.2 protein, another candidate protein indicated by the mass spectrometric analysis (Fig. 2C). In addition, recombinant RPL23A protein specifically stimulated the 7-39 hybridoma cells in a dose-dependent, class II major histocompatibility complex (MHC) I-A^d–dependent manner (Fig. 2D and fig. S12). Among 20-amino acid RPL23A peptides with consecutive overlapping of 5 amino acid residues, $RPL23A_{71\text{-}90}$ peptide stimulated 7-39 TCRs most potently (table S3 and fig. S13A).

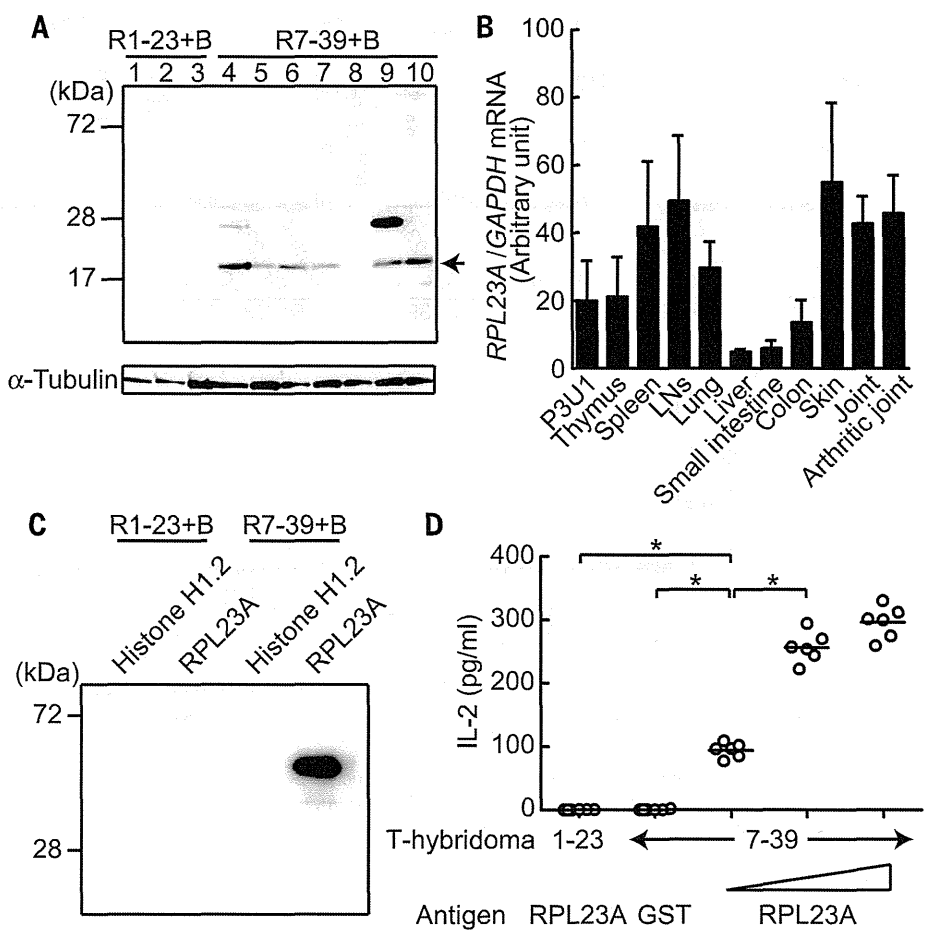

Fig. 2. Identification of the self antigen recognized by arthritogenic 7-39 TCRs. (**A**) Immunoblot analysis by sera from B cell–reconstituted R7-39 mice (n = 7) and B cell–reconstituted R1-23 mice (n = 3). Arrow indicates the commonly recognized protein. (**B**) Quantitative real-time polymerase chain reaction (qPCR) analysis for RPL23A gene expression in various tissues from SKG mice (n = 3). Error bars indicate means ± SD. (**C**) Recombinant RPL23A protein revealed by immunoblotting with sera from the indicated mice. (**D**) IL-2 production by 7-39 or 1-23 T cell hybridomas stimulated with the indicated recombinant proteins (n = 6). Horizontal bars indicate the means. *P < 0.05 (Kruskal-Wallis test followed by Steel-Dwass test). Results represent two [(A) to (C)] or three (D) independent experiments.

B cell–reconstituted R7-39 mice and arthritic SKG mice developed antibodies reacting with cyclic citrullinated peptides (CCP), as also observed in RA patients (*19*) (fig. S14A), yet there was no significant difference in titer of antibodies to RPL23A whether this was assessed with citrullinated or noncitrullinated RPL23A protein (fig. S14, B and C). In addition, the $RPL23A_{71\text{-}90}$ peptide recognized by 7-39 TCRs contained no arginine residue to be converted to citrulline (table S3).

Taken together, these results indicate that the ubiquitously expressed protein RPL23A can be a target antigen of both arthritis and dermatitis. Furthermore, more than one systemic antigen can be targeted for arthritis induction, because the 6-39 TCRs did not react to peptides derived from RPL23A (fig. S13B).

Upon transfer, $CD4^+$ T cells, but not sera, from B cell–reconstituted R7-39 mice induced arthritis in $Rag2^{-/-}$ mice (fig. S15). Indeed, $CD4^+$ T cells from arthritic joints or the regional lymph nodes of R7-39 mice produced inflammatory cytokines [including IL-17A, interferon-γ (IFN-γ), and granulocyte macrophage-colony stimulating factor (GM-CSF)] upon activation with phorbol 12-myristate 13-acetate (PMA) and ionomycin, RPL23A protein, or $RPL23A_{71\text{-}90}$ peptide (Fig. 3, A to D, fig. S16, A to D, and fig. S17). In addition, RPL23A stimulated nonarthritic SKG, but not BALB/c, $CD4^+$ T cells to produce IL-17A in vitro (Fig. 3E). It also augmented the production of IL-17A by $CD4^+$ T cells from SKG mice treated with mannan, which can trigger autoimmune arthritis in SKG mice by promoting T_H17 differentiation of arthritogenic $CD4^+$ T cells (*20*, *21*). An arthritic joint of SKG mice indeed harbored $CD4^+$ T cells possessing the Vβ CDR3 of 7-39 TCRs (table S2).

We next evaluated the contribution of T_{reg} cells to controlling arthritogenic $CD4^+$ T cells. T_{reg} cells

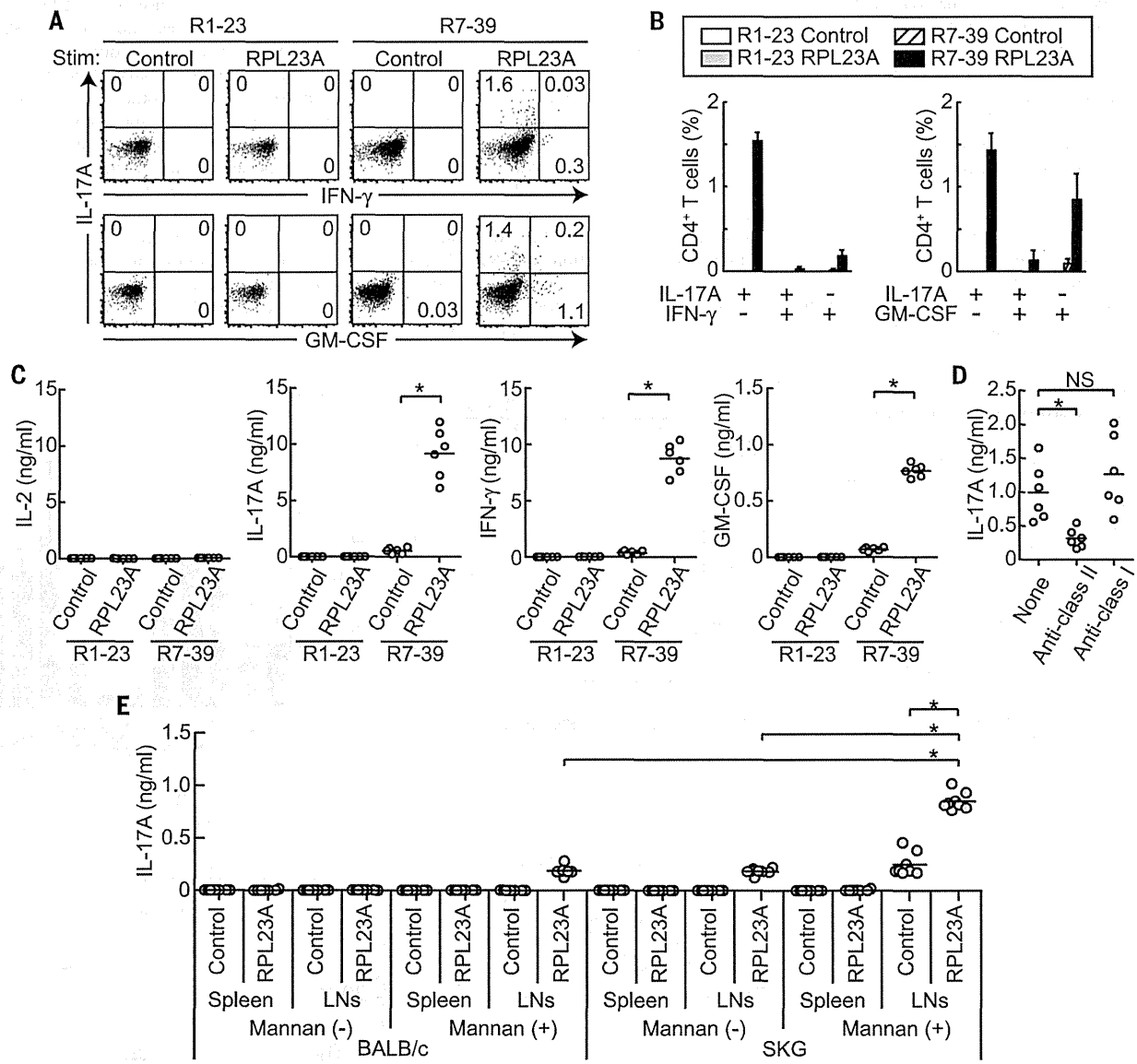

Fig. 3. RPL23A-reactive T_H cells in R7-39 mice. (**A**) Cytokine production by $CD4^+$ T cells from regional lymph nodes of R7-39 or R1-23 mice after in vitro stimulation with recombinant RPL23A or control glutathione *S*-transferase (GST) protein. Stim, stimulation. Data are representative of three independent experiments. (**B**) Percentages of cytokine-producing $CD4^+$ T cells in (A) (n = 3). (**C**) Cytokine amounts in culture supernatants in (A) (n = 6). (**D**) IL-17A production by RPL23A-stimulated lymphocytes from R7-39 mice in the presence or absence of blocking antibodies to MHC class I or class II (n = 6). (**E**) IL-17A production by lymphocytes stimulated with recombinant RPL23A or control GST proteins (n = 8). Lymphocytes were taken from SKG or BALB/c mice with or without mannan treatment. In (B), results are shown as means ± SD. In (C) to (E), horizontal bars indicate the means; *P < 0.05 (Kruskal-Wallis test followed by Steel-Dwass test); NS, not significant. Results represent two independent experiments in (B) and (C).

from either ZAP-70–intact BALB/c or ZAP-70–mutant SKG mice failed to suppress arthritis development in *Rag2*$^{-/-}$ mice when cotransferred with phenotypically activated or memory 7-39 TCR$^+$ CD4$^+$ T cells (figs. S7 and S18), although T_{reg} cells were capable of suppressing naïve arthritogenic T cells effectively (*9*).

These results collectively indicate that RPL23A is able to stimulate CD4$^+$ T cells in R7-39 mice via RPL23A-derived peptide–MHC class II complexes, driving them to differentiate into arthritogenic effector T_H cells (*20*), which are capable of mediating arthritis even in the presence of T_{reg} cells.

Lastly, we examined possible immune responses to RPL23A in RA patients. *RPL23A* mRNA was found to be ubiquitously expressed in healthy human tissues (Fig. 4A). In synovial tissues of RA patients and also in the apparently normal synovial tissues of osteoarthritis (OA) patients, RPL23A was detected in the cytoplasm of synovial cells, including CD55$^+$ FLSs (Fig. 4B). Relative to healthy controls (1.3%, n = 74), a significantly higher proportion of RA patients (16.8%, n = 374) were positive for serum immunoglobulin G–type autoantibodies to RPL23A (Fig. 4C). Two out of 23 psoriatic arthritis (PsA) patients (8.7%) were positive for the autoantibody, whereas all of the OA patients (n = 11), systemic lupus erythematosus (SLE) patients (n = 30), or

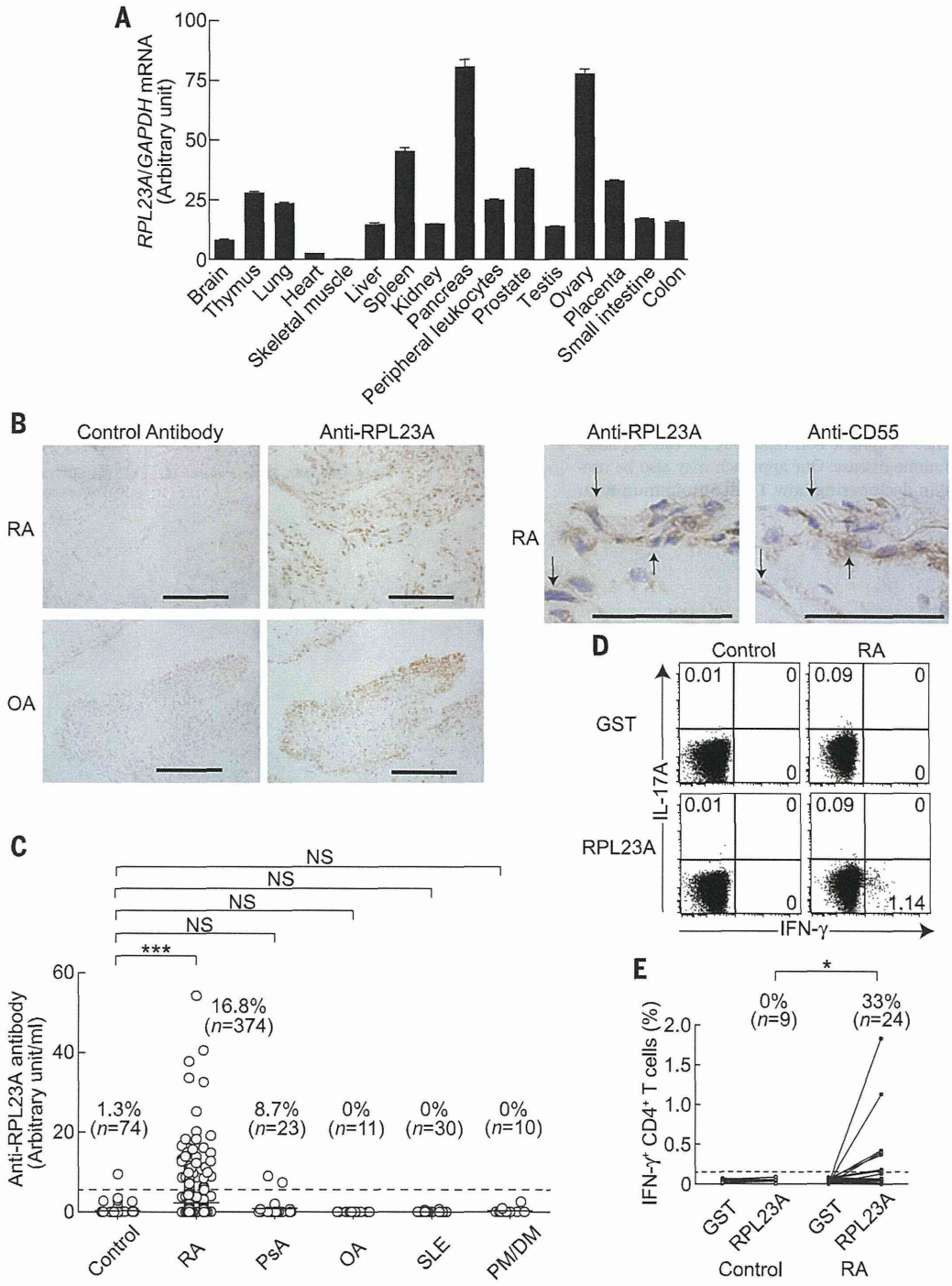

Fig. 4. Anti-RPL23A humoral and cellular immune responses in RA patients. (**A**) qPCR analysis of RPL23A gene expression in various tissues from healthy human subjects (n = 3). Results are shown as means ± SD and represent two independent experiments. (**B**) Immunohistochemical staining of synovial tissues from RA or OA patients for RPL23A or CD55 expression (scale bars, four images at left, 200 μm; two images at right, 50 μm). Serial sections were stained by anti-RPL23A, anti-CD55, or control antibody. Arrows indicate cells that are both RPL23A- and CD55-positive. Representative results from three patients are shown. (**C**) Serum levels of autoantibodies to RPL23A assessed by enzyme-linked immunosorbent assay (ELISA) in RA, PsA, OA, SLE, and PM/DM patients or healthy individuals. Horizontal bars indicate the medians. ***P < 0.001 (Kruskal-Wallis test followed by Dunn's multiple comparison test). (**D**) Cytokine production from CD4$^+$ T cells stimulated with recombinant RPL23A or GST protein. (**E**) Percentages of IFN-γ$^+$ cells in RPL23A- or GST-stimulated CD4$^+$ T cells in RA patients (n = 24) or healthy individuals (n = 9). *P < 0.05 (χ^2 test). Dashed lines indicate the threshold in (C) and (E).

polymyositis/dermatomyositis (PM/DM) patients (n = 10) were negative. In addition, in the synovial fluid of a subset of RA patients, we detected $CD4^+$ T cells producing IFN-γ upon stimulation with RPL23A (Fig. 4, D and E). These findings in humans, together with the key role of anti-RPL23A T cell responses for autoimmune arthritis and psoriasis-like dermatitis in mice, suggest that the responses may play a pathogenic role at least in a subset of patients with RA or PsA.

Our results show that by attenuating TCR signal intensity in developing T cells (hence reducing their sensitivity to thymic negative selection by natural self ligands), T cells reactive with ubiquitously expressed self antigens can be generated as dominant pathogenic clones causing systemic autoimmune disease. Because similar attenuation of TCR signaling at various degrees in conjunction with T_{reg} cell depletion is able to produce a variety of other autoimmune diseases in mice (*9*, *22*), this strategy of generating pathogenic T cells and characterizing the self antigens they recognize would facilitate our understanding of the mechanisms of other autoimmune diseases of currently unknown etiology. In addition, given that genetic polymorphism in a signaling molecule in T cells is a major determinant of genetic susceptibility to various human autoimmune diseases including RA (*23*), such a genetic variation might, at least in part, alter thymic selection, hence forming a TCR repertoire for causing autoimmune disease. Our approach may also be useful in deciphering how T cell autoimmunity to a ubiquitous self antigen triggers localized tissue damage in RA and other human autoimmune diseases, and in devising effective means of systemic or local intervention in the disease process.

REFERENCES AND NOTES

1. S. Sakaguchi, F. Powrie, R. M. Ransohoff, *Nat. Med.* **18**, 54–58 (2012).
2. P. Marrack, J. Kappler, B. L. Kotzin, *Nat. Med.* **7**, 899–905 (2001).
3. M. Feldmann, F. M. Brennan, R. N. Maini, *Cell* **85**, 307–310 (1996).
4. G. S. Firestein, *Nature* **423**, 356–361 (2003).
5. I. B. McInnes, G. Schett, *N. Engl. J. Med.* **365**, 2205–2219 (2011).
6. C. X. Chang *et al.*, *Front. Biosci.* **16**, 3014–3035 (2011).
7. L. Y. Hsu, Y. X. Tan, Z. Xiao, M. Malissen, A. Weiss, *J. Exp. Med.* **206**, 2527–2541 (2009).
8. N. Sakaguchi *et al.*, *Nature* **426**, 454–460 (2003).
9. S. Tanaka *et al.*, *J. Immunol.* **185**, 2295–2305 (2010).
10. C. L. Sommers *et al.*, *Science* **296**, 2040–2043 (2002).
11. O. M. Siggs *et al.*, *Immunity* **27**, 912–926 (2007).
12. J. Holst *et al.*, *Nat. Protoc.* **1**, 406–417 (2006).
13. G. P. Lennon *et al.*, *Immunity* **31**, 643–653 (2009).
14. M. L. Bettini, M. Bettini, M. Nakayama, C. S. Guy, D. A. Vignali, *Nat. Protoc.* **8**, 1837–1840 (2013).
15. See supplementary materials on *Science* Online.
16. F. O. Nestle, D. H. Kaplan, J. Barker, *N. Engl. J. Med.* **361**, 496–509 (2009).
17. K. Suzuki, I. G. Wool, *J. Biol. Chem.* **268**, 2755–2761 (1993).
18. W. Fan, M. Christensen, E. Eichler, X. Zhang, G. Lennon, *Genomics* **46**, 234–239 (1997).
19. W. J. van Venrooij, J. J. van Beers, G. J. Pruijn, *Nat. Rev. Rheumatol.* **7**, 391–398 (2011).
20. K. Hirota *et al.*, *J. Exp. Med.* **204**, 41–47 (2007).
21. M. Hashimoto *et al.*, *J. Exp. Med.* **207**, 1135–1143 (2010).
22. M. Ono, J. Shimizu, Y. Miyachi, S. Sakaguchi, *J. Immunol.* **176**, 4748–4756 (2006).
23. N. Bottini, T. Vang, F. Cucca, T. Mustelin, *Semin. Immunol.* **18**, 207–213 (2006).

ACKNOWLEDGMENTS

We thank D. O. Adeegbe, Y. Kitagawa, and K. Chen for critical reading of the manuscript; E. Yamamoto, M. Matsuura, R. Ishii, Y. Tada, Y. Funabiki, the technical support team (Graduate School of Medicine, Kyoto University), and K. Saito of DNA-chip Development Center for Infectious Diseases (RIMD, Osaka University) for technical assistance; T. Matsushita for histology; T. Kitamura for gifts of the packaging cell line Plat-E; the members of the Department of Rheumatology and Clinical Immunology, Kyoto University, for providing us with patients' sera; and the members of our laboratories for comments. The data presented in this paper are tabulated in the main paper and in the supplementary materials. eFOX mice and plasmids for making retrogenic mice are subject to a material transfer agreement. A patent application related to the work in this paper has been filed (PCT/JP2014/069306: A way to diagnose autoimmune arthritis; Y.I. and S.S. as inventors). Supported by Grants-in-Aid for Specially Promoted Research 20002007 (S.S. and Y.I.),;for Young Scientists (B) 24790996 (Y.I.) from the Japan Society for the Promotion of Science; Core Research for Evolutional Science and Technology from the Japan Science and Technology Agency (S.S.); NIH grant R01 DK089125 (D.A.A.V.); and American Lebanese Syrian Associated Charities (D.A.A.V.). M.H., T.F., M.F., H.I., and T.M. are affiliated with a department that is supported financially by five pharmaceutical companies (Mitsubishi Tanabe Pharma Co., Bristol-Myers K.K., Chugai Pharmaceutical Co. Ltd., AbbVie GK., and Eisai Co. Ltd.). The sponsors were not involved in the study design; in the collection, analysis, or interpretation of data; in the writing of this manuscript; or in the decision to submit the article for publication.

SUPPLEMENTARY MATERIALS

www.sciencemag.org/content/346/6207/363/suppl/DC1
Materials and Methods
Supplementary Text
Figs. S1 to S18
Tables S1 to S3
References (*24*–*36*)

22 July 2014; accepted 16 September 2014
10.1126/science.1259077

Detection of T cell responses to a ubiquitous cellular protein in autoimmune disease

Yoshinaga Ito *et al.*

Science **346**, 363 (2014);
DOI: 10.1126/science.1259077

OPEN ACCESS Freely available online

PLOS ONE

MCP/CCR2 Signaling Is Essential for Recruitment of Mesenchymal Progenitor Cells during the Early Phase of Fracture Healing

Masahiro Ishikawa[1,2], Hiromu Ito[1]*, Toshiyuki Kitaori[1], Koichi Murata[1], Hideyuki Shibuya[1], Moritoshi Furu[1,2], Hiroyuki Yoshitomi[3], Takayuki Fujii[1], Koji Yamamoto[4], Shuichi Matsuda[1]

1 Department of Orthopaedic Surgery, Kyoto University Graduate School of Medicine, Kyoto, Japan, **2** Department of the Control for Rheumatic Disease, Kyoto University Graduate School of Medicine, Kyoto, Japan, **3** The Center for Innovation in Immunoregulative Technology and Therapeutics, Kyoto University Graduate School of Medicine, Kyoto, Japan, **4** Center for the Promotion of Interdisciplinary Education and Research, Kyoto University, Kyoto, Japan

Abstract

Objective: The purpose of this study was to investigate chemokine profiles and their functional roles in the early phase of fracture healing in mouse models.

Methods: The expression profiles of chemokines were examined during fracture healing in wild-type (WT) mice using a polymerase chain reaction array and histological staining. The functional effect of monocyte chemotactic protein-1 (MCP-1) on primary mouse bone marrow stromal cells (mBMSCs) was evaluated using an *in vitro* migration assay. MCP-1$^{-/-}$ and C-C chemokine receptor 2 (CCR2)$^{-/-}$ mice were fractured and evaluated by histological staining and micro-computed tomography (micro-CT). RS102895, an antagonist of CCR2, was continuously administered in WT mice before or after rib fracture and evaluated by histological staining and micro-CT. Bone graft exchange models were created in WT and MCP-1$^{-/-}$ mice and were evaluated by histological staining and micro-CT.

Results: *MCP-1* and *MCP-3* expression in the early phase of fracture healing were up-regulated, and high levels of MCP-1 and MCP-3 protein expression observed in the periosteum and endosteum in the same period. MCP-1, but not MCP-3, increased migration of mBMSCs in a dose-dependent manner. Fracture healing in MCP-1$^{-/-}$ and CCR2$^{-/-}$ mice was delayed compared with WT mice on day 21. Administration of RS102895 in the early, but not in the late phase, caused delayed fracture healing. Transplantation of WT-derived graft into host MCP-1$^{-/-}$ mice significantly increased new bone formation in the bone graft exchange models. Furthermore, marked induction of MCP-1 expression in the periosteum and endosteum was observed around the WT-derived graft in the host MCP-1$^{-/-}$ mouse. Conversely, transplantation of MCP-1$^{-/-}$ mouse-derived grafts into host WT mice markedly decreased new bone formation.

Conclusions: MCP-1/CCR2 signaling in the periosteum and endosteum is essential for the recruitment of mesenchymal progenitor cells in the early phase of fracture healing.

Citation: Ishikawa M, Ito H, Kitaori T, Murata K, Shibuya H, et al. (2014) MCP/CCR2 Signaling Is Essential for Recruitment of Mesenchymal Progenitor Cells during the Early Phase of Fracture Healing. PLoS ONE 9(8): e104954. doi:10.1371/journal.pone.0104954

Editor: Federico Quaini, University-Hospital of Parma, Italy

Received May 14, 2014; **Accepted** July 14, 2014; **Published** August 18, 2014

Data Availability: The authors confirm that all data underlying the findings are fully available without restriction. All relevant data are within the paper and its Supporting Information files.

Funding: This work was supported by Grant-in-Aids from the Ministry of Education of Japan (No. 19591756, 21591942). The funders had no role in study design, data collection and analysis, decision to publish, or preparation of the manuscript.

Competing Interests: The authors have declared that no competing interests exist.

* Email: hiromu@kuhp.kyoto-u.ac.jp

Introduction

The prevalence of osteoporosis is increasing with the aging of society. In particular, osteoporotic fractures are a major public health problem with a low one-year patient's survival rate [1,2]. Management of the fracture is difficult because of poor bone quality, and there is a high risk of fixation failure and nonunion. To avoid these difficulties, numerous attempts have been made to develop techniques to improve fracture healing, including addition or injection of bone-forming factors or cells such as mesenchymal stem/progenitor cells [3,4]. However, treatment options remain below expectations despite vigorous attempts to find new useful therapies. One major reason is that the mechanisms responsible for fracture healing are complex and not fully understood. Hence, elucidating the mechanisms involved in fracture healing is fundamental to developing novel therapeutic strategies to improve fracture healing.

Normal fracture healing follows a unique, distinct healing process, which can be divided into three overlapping phases: inflammation, repair and remodeling [5]. Among these three phases, the repair and remodeling phases largely recapitulate the process of normal bone development [6]. In contrast, the inflammation phase is a unique process that is not observed in

the organogenesis of bone and develops after birth to induce bone repair. Previous studies have shown that inflammation plays a pivotal role in fracture healing [7,8] and that mesenchymal stem/progenitor cells are systemically or locally recruited to the fracture site in the early inflammatory phase [5,9]. Many proinflammatory cytokines and chemokines are released from the fracture site in the early inflammatory phase [9,10]. Chemokines are small, chemoattractant cytokines that play key roles in the recruitment of leukocytes to sites of inflammation and injury. Studies have shown that stem/progenitor cell migration and organ-specific recruitment are regulated by chemokines and their receptors [11–13]. In addition, mesenchymal stem/progenitor cells express a variety of chemokine receptors [14], and chemokine-mediated mesenchymal stem/progenitor cell migration has been shown *in vitro* and *in vivo* [15,16].

Over the past decade, attention has focused on stem/progenitor cells because of their pivotal role in tissue regeneration. Mesenchymal stem/progenitor cells exhibit extensive tropism for tissue injury sites [17]. These cells differentiate into mesenchymal lineage cells when exposed to appropriate environmental cues and can promote tissue repair of many organs, including bone. In addition, mesenchymal stem/progenitor cells appear to exist in almost all tissues, including bone marrow, muscle and the periosteum, and if not present, can reach tissues via the blood circulation [18]. Therefore, mesenchymal stem/progenitor cells can be recruited from the circulation or surrounding tissues and participate in the repair of the injured organs [12,19].

Several studies have shown that systemically infused mesenchymal stem/progenitor cells can migrate to, and participate in, the repair of injured tissue [20–22]. We have previously demonstrated in a bone graft model that stromal cell-derived factor-1 (SDF-1) is induced in the periosteum of fracture sites and promotes endochondral bone repair by recruiting C-X-C chemokine receptor 4 (CXCR4)-expressing mesenchymal stem/progenitor cells [23]. Thus, mesenchymal stem/progenitor cell therapy may be a novel therapeutic strategy to improve fracture healing. To develop an efficient therapy, it is crucial to elucidate the precise mechanisms for recruitment of mesenchymal stem/progenitor cells to the fracture site. However, these mechanisms, especially during the early inflammatory phase, are largely unknown.

To identify the factor(s) essential for normal fracture healing, we used a polymerase chain reaction (PCR) array and mouse rib fracture model in which cell potential is non-impaired by surgical intramedullary fixation. We also used an exchange-graft model to show gain- or loss-of-function. We demonstrate herein that the expression level of monocyte chemotactic protein-1 (MCP-1) is up-regulated exclusively in the early fracture phase and that MCP-1 is expressed at the periosteum and endosteum of the fractured bones. Gain- and loss-of-function studies showed that the MCP-1/C-C chemokine receptor 2 (CCR2) axis is crucial in the early phase of fracture healing. In summary, these results indicate that the MCP-1/CCR2 axis provides essential signaling for normal bone healing and may be a novel, potent therapeutic target for fracture healing.

Materials and Methods

Reagents

Recombinant mouse MCP-1 and MCP-3 were purchased from Abcam (Cambridge, MA, USA). CCR2 antagonist (RS102895) was purchased from Sigma (St. Luis, MO, USA).

Mouse rib fracture model

All animal studies were conducted in accordance with principles and procedures approved by the Kyoto University Committee of Animal Resources. Surgeries were undergone under anesthesia with diethylether, and mice were euthanatized with cervical dislocation upon sacrifice. Mouse rib fracture models were created using 6-week-old C57BL/6 wild-type (WT), MCP-1$^{-/-}$ and CCR2$^{-/-}$ mice, as described previously [24]. Five mice from each fracture group were sacrificed 0, 1, 2, 3, 5, 7, 10, 14, 21, and 25 days after fracture. To evaluate the inhibitory effect of the receptor antagonist, the mice received continuous administration of the selective CCR2 antagonist, RS102895. RS102895 was dissolved in dimethyl sulfoxide (DMSO) and via an osmotic pump (model 1002; Durect, Cupertino, CA, USA), was delivered to a total of 10 mg/kg/day, beginning 2 days before or 4 days after rib fracture, and until day 12. In the control group, DMSO alone was administered for 14 days.

Femoral segmental bone graft transplantation model

A mouse segmental bone graft model was created using 6-week-old C57BL/6 WT and MCP-1$^{-/-}$ mice as described previously [25]. Briefly, 4-mm of mid-diaphyseal segmental bone was removed from the femur of the donor mouse. The graft was dissected carefully to remove the muscle and bone marrow without compromising the periosteum, and segmental bone derived from a WT or MCP-1$^{-/-}$ mouse was transplanted immediately into a 4-mm segmental defect in a host WT or MCP-1$^{-/-}$ mouse. Four groups of segmental bone graft models were used: MCP-1$^{-/-}$ donor to MCP-1$^{-/-}$ host [knockout (KO)-to-KO], WT donor to MCP-1$^{-/-}$ host (WT-to-KO), WT donor to WT host (WT-to-WT), and MCP-1$^{-/-}$ donor to WT host (KO-to-WT). The bone graft was stabilized using a 25 G stainless pin placed through the intramedullary marrow cavity, and the mice were sacrificed on day 21 after the surgery for RNA extraction and histological analysis.

Micro-CT analysis

Mice were sacrificed postoperatively for micro-computed tomography (micro-CT) imaging on days 7 (femoral bone graft model) and 21 (rib fracture model). The rib and femur were scanned using a micro-CT system (SMX-100CT-SV3; Shimadzu, Tokyo, Japan) at 2400 views, five frames per view, 40 kV, and 40 μA. Three-dimensional (3D) images were rendered and evaluated using VG Studio MAX (Nihon Visual Science Software, Tokyo, Japan). The newly formed callus was spatially segmented from the native cortical bone in the two-dimensional (2D) tomograms, the 3D images of the callus were rendered, and the total volume was measured on the digitally extracted callus tissue. The newly formed calluses in a region of interest covering the entire length of the bone graft, including 1 mm of the host bone at both proximal and distal bone graft junctions, were analyzed to determine bone graft healing.

RNA extraction, quantitative real-time PCR and PCR array

Total RNA was extracted from mouse rib and femoral bone graft specimens as described previously [26]. A PCR array was performed to measure mRNA levels for chemokines during the fracture healing process. Two micrograms of RNA was processed using an RT2 First Strand Kit (SA Biosciences, Frederick, MD, USA) according to the manufacturer's specifications. Quantitative PCR analysis for chemokines and receptors was assessed using a chemokine array (Chemokines & Receptors PCR Array, Mouse, PAMM-022, SA Biosciences). We analyzed the data using the RT2 profiler PCR Array Data Analysis software (SA Biosciences). The change in gene expression level determined by PCR array analysis was confirmed by quantitative real-time PCR. All gene

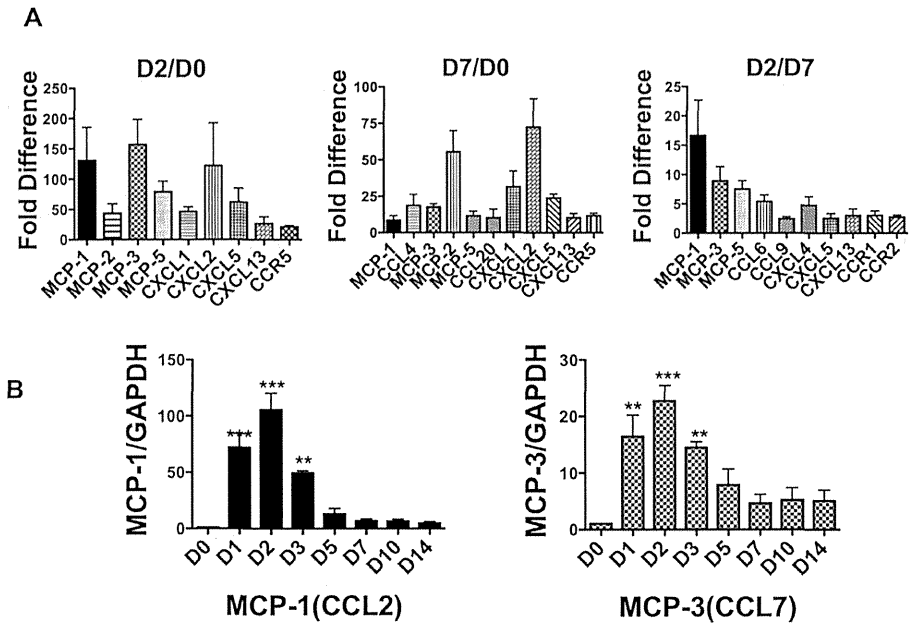

Figure 1. The expression profiles of chemokines and their receptors during fracture healing. Expression levels during fracture healing were examined using a rib fracture model. **A**: PCR array data for up-regulated chemokines and their receptors during fracture healing are shown. Expression levels were compared between days 0 and 2, days 0 and 7, and days 2 and 7. **B**: Time course of *MCP-1* and *MCP-3* mRNA expression in a rib fracture model, as analyzed by real-time PCR. Expression levels are the fold change from day 0 levels. Values are means ± SEM of more than four separate experiments. $^{**}P<0.01$ $^{***}P<0.001$ compared with the day 0 group.
doi:10.1371/journal.pone.0104954.g001

expression data were normalized against glyceraldehyde phosphate dehydrogenase (GAPDH).

Histological analysis

Rib and femur specimens were processed as paraffin-embedded sections and stained with hematoxylin and eosin and were subjected to immunohistochemical analyses as described previously [23,24].

In vitro chemotaxis assay

In vitro cell migration of primary mouse bone marrow stromal cells (mBMSCs) (1.0×10^5 cells/100 μl) was assessed using Transwell inserts with an 8-μm pore membrane, as described previously [23]. For the chemotaxis assay, different concentrations of MCP-1 or MCP-3 (0, 10, or 100 ng/ml) in 500 μl of medium were applied to the lower chambers. For the inhibition assay, RS102895 (400 nM) was also applied to the lower chambers. After 24 h of incubation, the migrated cells were counted under light microscopy.

Primary cell culture, cell line, osteogenesis and chondrogenesis assay

For the osteogenesis assay, mBMSCs were harvested and cultured as described previously [23]. mBMSCs were cultured with osteogenic base media (R&D Systems, Minneapolis, MN, USA) for 2 days. On reaching 70% confluence, the medium was replaced with osteogenic differentiation medium and was changed every 3 days thereafter. In some experiments, recombinant mouse MCP-1 (200 ng/ml) was added every 3 days with each medium change. On day 14 after plating, cells were harvested for alizarin red staining and gene expression analysis. For the chondrogenesis assay, ATDC5 cells were cultured and maintained in Dulbecco's Modified Eagles Medium (DMEM) and Ham's F-12 at a 1:1 ratio with 5% fetal bovine serum (FBS) supplemented with insulin (10 mg/mL, Sigma), transferrin (5.5 mg/mL, Sigma), and sodium selenite (5 ng/mL, Sigma) to induce chondrocyte differentiation as described previously [27]. The medium was changed every 2 days thereafter. In some experiments, MCP-1 (0, 20, 100 or 200 ng/ml) was simultaneously added every 2 days with the medium change. On day 28 after plating, cells were harvested for gene expression analysis.

Statistical analysis

Data are presented as means ± standard error of the mean (SEM). We analyzed the data using GraphPad Prism Version 5.00 (GraphPad software). Statistical comparisons between two groups were performed using a Student's two-tailed *t* test. Differences between three groups were analyzed using the Bonferroni method. *P* values <0.05 were considered significant.

Results

Chemokine expression profile in the early phase of fracture healing

We first used PCR array to investigate the expression profile of chemokines during fracture healing in the WT mouse rib fracture model. The PCR array analysis showed that the expression levels of *MCP-1* and *MCP-3* were significantly higher on day 2 compared with days 0 and 7 (Figure 1A). *MCP-1* and *MCP-3* expression levels were more than 100 times higher on day 2 than on day 0. *MCP-1* and *MCP-3* expression levels on day 2 were five times higher than those on day 7. To confirm the PCR array data, we next examined the gene expression levels for *MCP-1* and

MCP-3 during the fracture healing process. Consistent with the PCR array analysis, the expression of *MCP-1* and *MCP-3* increased during the early phase of fracture healing (Figure 1B). *MCP-1* and *MCP-3* were expressed on day 1 and their expression peaked on day 2. By day 7, expression of both genes had declined markedly.

In vivo expression of MCP-1 during the early inflammatory phase of fracture healing

Because CCR2 is the major and common receptor for MCP-1 and MCP-3, we focused on the expression of MCP-1, MCP-3 and CCR2 in fracture healing, especially during the early inflammatory phase. To confirm the localization of MCP-1, MCP-3 and CCR2 expression during the early inflammatory phase of fracture healing, we used immunohistochemistry to examine rib fracture healing in WT mice. Low expression levels of MCP-1 and MCP-3 were observed at the periosteum in the unfractured rib, (Figures S1A, B) and high levels of MCP-1 and MCP-3 protein were observed at the periosteum and endosteum on day 3 in the fractured rib (Figure 2A, B). Conversely, little or no CCR2 staining was detected in the unfractured rib (Figure S1C), and on day 3, CCR2-positive cells were found predominantly within the bone marrow and surrounding tissues (Figure 2C).

MCP-1 induces mBMSCs migration *in vitro*

To examine the functional roles of MCP-1 and MCP-3 signaling in fracture healing, we first examined whether MCP-1 and MCP-3 could induce the migration of mBMSCs. MCP-1 significantly increased mBMSC migration in a dose-dependent manner, whereas MCP-3 did not (Figure 3A). Because MCP-1 and MCP-3 act through their receptor CCR2, we examined the expression of CCR2 in these cells. Consistent with a previous report [30], RT-PCR analysis showed that CCR2 was expressed in mBMSCs (Figure 3B). We also examined whether CCR2 mediates MCP-1-induced migration of mBMSCs. RS102895 (400 nM) effectively inhibited the MCP-1-induced migration of mBMSCs (Figure 3A). Because MCP-3 did not affect migration of the cells, we therefore focused on MCP-1. To further investigate possible roles of MCP-1, we next examined osteogenic differentiation of mBMSCs in response to MCP-1. Isolated mBMSCs were capable of spontaneously differentiating into alizarin red-positive cells and showed increased levels of *Runx2*, *osterix* and *alkaline phosphatase (ALP)* in the osteoinduction media on day 14. However, alizarin red staining revealed no difference between osteoinduced mBMSCs with or without MCP-1 (Figure S2A). Similarly, no difference in the gene expression of *Runx2, osterix, or ALP* was observed in cells treated with or without MCP-1 (Figure S2A). Because MCP-1 did not affect the osteogenic differentiation of mBMSCs, we also examined whether MCP-1 affects chondrogenic differentiation using ATDC5 cells *in vitro*. Alcian blue staining showed that the presence of MCP-1 was not associated with any obvious differences in cells treated with or without MCP-1 on day 28. Moreover, *SOX9, Col-2* and *Col-10* showed similar expression patterns in cells treated with or without MCP-1 (Figure S2B).

In vivo roles of MCP-1 and CCR2 during the early inflammatory phase of fracture healing

To investigate the functional roles of MCP-1 and CCR2 in fracture healing, rib fracture healing was assessed in WT and KO mice. Fracture calluses were examined by micro-CT and histological analysis. Histological analyses showed a smaller proportion of cartilage in the callus in MCP-$1^{-/-}$ mice compared with WT mice on day 7 (Figure S3A). By day 21, fractures had healed in the WT mice and cartilage was almost completely replaced by bone in the callus (Figure 4A). Conversely, the healing processes progressed incompletely in MCP-$1^{-/-}$ and CCR$2^{-/-}$ mice by day 21, and the central area of the cartilaginous callus remained (Figure 4A). By day 25, a bridging callus was apparent in MCP-$1^{-/-}$ and CCR$2^{-/-}$ mice, and was similar in appearance to that observed in WT mice on 21 day (Figure S3B). The callus volume was significantly smaller in both MCP-$1^{-/-}$ and CCR$2^{-/-}$ mice than in WT mice on day 21 (Figure 4B, C).

Next, to elucidate whether the MCP-1/CCR2 axis is involved during the early phase of fracture healing, we continuously administered RS102895 before (pre-treatment) or after (post-treatment) rib fracture. Micro-CT analysis showed delayed fracture healing in the pre-treatment group compared with both the control and post-treatment groups. On day 21, the callus volume was significantly smaller in the pre-treatment group than in the control and post-treatment groups (Figures 5A, B). Histological analysis showed that fractures in both the control and post-treatment groups had healed by day 21 and that cartilaginous tissue was absent in the callus. Conversely, less cartilaginous tissue was observed in the callus in the pre-treatment group on day 7 (Figure 5C), and cartilaginous tissue in a central area of the callus was observed on day 21 (Figure S3C). These results indicate that the MCP-1/CCR2 axis is an essential component during the early phase of fracture healing.

Periosteal bone formation in grafts from WT mice implanted into MCP-1-deficient mice: gain-of-function

To examine the roles of MCP-1 at the periosteum and endosteum during fracture healing, we performed gain-of-function studies using a segmental bone graft transplantation model. A segmental bone graft was transplanted from an MCP-$1^{-/-}$ mouse to another MCP-$1^{-/-}$ mouse (KO-to-KO). Micro-CT and histological analysis were used to quantify new bone formation on day 21. Radiologic and micro-CT analyses showed that KO-to-KO transplantation caused a delay in fracture healing on day 21 (Figure 6A). Minimal periosteal bone formation was observed along the surface of the bone graft because of the lack of periosteal bone formation. We next created bone graft exchanging models between MCP-$1^{-/-}$ and WT mice, in which a segmental bone derived from a WT mouse was transplanted into a host MCP-$1^{-/-}$ mouse (WT-to-KO). In contrast to KO-to-KO bone graft transplantation, transplantation of the WT-derived graft into the host KO mouse significantly increased new bone formation and led to marked recovery of periosteal bone formation on day 21 (Figures 6A, B). Histological analysis further revealed marked and localized induction of MCP-1 expression in the callus and endosteum around the WT-derived graft in the host MCP-$1^{-/-}$ mouse (Figure 6C). By contrast, no MCP-1 expression was observed in the callus and endosteum of the host bone in the same section.

Reduction in periosteal bone formation in grafts from MCP-1-deficient mice implanted into WT mice: loss-of-function

To confirm whether MCP-1 is a crucial chemokine in the fracture healing process, we performed loss-of-function studies using WT-to-WT and KO-to-WT bone graft models. Transplantation of a WT donor graft into a WT host mouse led to abundant new bone formation and a bridging callus around the WT-derived graft on day 21 (Figures 6D, E). By contrast, transplantation of a KO-derived graft into a WT host markedly reduced the amount of periosteal bone formation in the donor graft.